Quantitative in situ proximity ligation assays examining protein interactions and phosphorylation during smooth muscle contractions.

Yeming Xie and **Brian A. Perrino**[*]

Department of Physiology and Cell Biology, University of Nevada Reno, School of Medicine, MS 0352, 1664 N Virginia St, Reno, NV 89557, USA.

Abstract

Antibody-based in situ proximity ligation assays (isPLA) have the potential to study protein phosphorylation and protein interactions with spatial resolution in intact tissues. However, the application of isPLA at the tissue level is limited by a lack of appropriate positive and negative controls and the difficulty in accounting for changes in tissue shape. Here we demonstrate a set of experimental and computational approaches using gastric fundus smooth muscles to improve the validity of quantitative isPLA. Appropriate positive and negative biological controls and PLA technical controls were selected to ensure experimental rigor. To account for changes in morphology between relaxed and contracted smooth muscles, target PLA spots were normalized to smooth muscle myosin light chain 20 PLA spots or the cellular cross-sectional areas. We describe the computational steps necessary to filter out false-positive improperly sized spots and set the thresholds for counting true positive PLA spots to quantify the PLA signals. We tested our approach by examining protein phosphorylation and protein interactions in smooth muscle myofilament Ca^{2+} sensitization pathways from resting and contracted gastric fundus smooth muscles. In conclusion, our tissue-level isPLA method enables unbiased quantitation of protein phosphorylation and protein-protein interactions in intact smooth muscle tissues, suggesting the potential for quantitative isPLA applications in other types of intact tissues.

Keywords

Muscle Contraction; Muscle, Smooth; Phosphorylation; Contractile Proteins; Integrins; Proximity Ligation Assay

Conflicts of Interest

The authors disclose no conflicts.

Subject Category

Enzymatic assays and analysis

1. INTRODUCTION

Many proteins require reversible post-translational modifications and interactions with other proteins or molecules to properly function [1, 2]. Protein-protein interactions, protein complex composition, and protein phosphorylation are constantly changing depending upon the ongoing physiological demands of cells and tissues [3]. In addition to quantifying protein abundance, it is also important to determine whether a protein contains post-translational modifications, is present in a complex with other proteins, in which cells is it expressed, and in which subcellular compartments the different states of the protein are present. The in situ proximity ligation assay (isPLA) has emerged as a powerful tool to characterize proteins and their interactions in any cell or tissue [4, 5]. Traditional biochemical assays (western blot, co-immunoprecipitation, ELISA) to study protein phosphorylation and protein-protein interactions are based on protein extraction procedures which may result in loss of functional compartmentalization and non-physiological aggregation and interactions [6, 7]. isPLA of fixed tissue sections or cells, on the other hand, preserves internal structures and their spatial organization to enable detection and quantitation of protein phosphorylation and protein-protein interactions that are more reflective of the native cell and tissue [8].

Smooth muscle contraction requires phosphorylation of the 20kDa myosin light chain (**LC20**) for cross-bridge formation between actin and myosin [9, 10]. Regulation of LC20 phosphorylation by myosin light chain kinase (**MYLK**) and myosin light chain phosphatase (**MLCP**) is the primary determinant of the strength of contractions at a given level of $[Ca^{2+}]_i$ [11]. Smooth muscles generate greater force for a given increase in $[Ca^{2+}]_i$ by activating protein kinase C (**PKC**) and Rho-associated kinase 2 (**ROCK2**) to phosphorylate protein kinase C-potentiated inhibitor protein of 17kDa (**CPI-17**) and myosin phosphatase targeting subunit (**MYPT1**) to inhibit MLCP and increase LC20 phosphorylation [12, 13]. Basal CPI-17 and MYPT1 phosphorylation establishes the basal sensitivity of gastric muscles to excitatory stimuli [10, 14, 15]. In addition to cytoplasmic kinases and phosphatases, a number of reports have demonstrated that dynamic interactions between contractile proteins and focal adhesions are important for smooth muscle contraction [16–18]. Tyrosine phosphorylation and activation of protein tyrosine kinase 2β (**Pyk2**) or focal adhesion kinase (**FAK**), along with the recruitment of other integrin-associated proteins to focal adhesions, occurs during contraction and force development [17, 19, 20]. We showed that mechanical force or tension is sufficient to activate FAK, and that FAK is involved in the activation of the PKC–CPI-17 Ca^{2+} sensitization pathway in gastric fundus smooth muscles, suggesting that myofilament Ca^{2+} sensitization mechanisms play a role in myofilament function at focal adhesions [21]. These actin filament modifications and remodeling are thought to facilitate the polymerization of cortical cytoskeletal actin filaments to increase the stability of focal adhesions in the membrane, allowing for the force generated by actin

filaments attached to the cytoplasmic domains of β1integrin by talin to be transmitted to the connective tissue of the extracellular matrix [22–25].

Numerous studies, including our own, have utilized SDS-PAGE and western blotting techniques to measure changes in phosphorylation of these regulatory proteins, to demonstrate the importance of these myofilament sensitizing mechanisms for smooth muscle contractions [14, 15, 26–29]. Co-immunoprecipitation **(Co-IP)** approaches have also revealed a number of interactions between contractile proteins and focal adhesions in smooth muscles [30–34]. However, due to their range of sensitivities, SDS-PAGE/western blotting and co-IP approaches typically require a large amount of starting material to yield measurable assays of protein levels, phosphorylation, and protein-protein interactions [8, 35]. For smooth muscle tissues in which small amounts of starting material are unavoidable (e.g. murine pylorus, gastric fundus or antrum, ureter, oviduct), isPLA may provide an effective alternative method for measuring functional changes in protein-protein interactions and protein phosphorylation [5, 36].

Currently, isPLA signals in tissue sections or monolayer cell cultures are quantified as spots per cell or nucleus, or signal intensity per unit image area [35, 37–39]. However, these quantitation methods are not suitable for measuring changes in protein-protein interactions or protein phosphorylation in tissues composed of elongated cells which can undergo dramatic morphological changes in response to external stimuli, such as smooth muscles. In cross-sections from intact smooth muscles in which individual smooth muscle cells display an elongated spindle shape, there is not always a 1:1 ratio of nuclei:cells in the region of interest. In addition, the smooth muscle tissue and smooth muscle cell morphologies may significantly change during contraction and relaxation [40]. Changes in cell lengths and diameters will lead to a change in cell density within the region being imaged, which makes it more difficult to compare the PLA spot counts of sample tissues from different treatments without proper normalization.

In this report we demonstrate methods to optimize the use of isPLA in smooth muscle tissue sections. In addition to specifying isPLA technical controls, we identified PLA antibody pairs for positive and negative biological controls that correlate with biochemical data from previous studies. We optimized the PLA spot counting method with Fiji to exclude PLA noise [41]. Instead of normalizing the PLA signals to the number of nuclei, we evaluated two different methods for isPLA signal normalization. We used the cellular cross-sectional areas or the spot count from LC20/LC20 single-protein PLA as novel internal controls; after determining that these parameters did not change during isometric contractions of the smooth muscles. Single protein LC20/LC20 PLA was done by using two LC20 antibodies from different host species that recognize different epitopes on LC20, to quantify the number of LC20 PLA spots. We then utilized isPLA to determine its feasibility for measuring changes in protein phosphorylation and protein-protein interactions in response to a contractile stimulus. Our data shows that measuring isometric contractile responses minimizes changes in muscle length, allowing cellular cross-sectional areas or the LC20/LC20 PLA spot counts to be used as internal controls for measuring the protein phosphorylation or protein-protein interaction PLA spot counts from relaxed and contracted smooth muscles. We show that changes in MYPT1, CPI-17, and LC20 phosphorylation, and

changes in the association between Ca^{2+} sensitization proteins, β1integrin, and FAK, can be detected and quantitated by isPLA of smooth muscle cross-sections. Our findings validate isPLA methodology for studying changes in protein phosphorylation, and protein-protein interactions in smooth muscle tissues during *ex vivo* contractile responses, and may lead to wider applications of isPLA in smooth muscle physiology studies.

2. MATERIALS AND METHODS

2.1 Ethical approval.

All animal care and experimental procedures complied with the National Institutes of Health Guide for the Care and Use of Laboratory Animals and were approved by the University of Nevada, Reno Institutional Animal Care and Use Committee. Mice (C57BL/6; 6 to 8 weeks old; male; 20–30 g) were obtained from Charles River Laboratories (Hollister, CA, USA). The mice were housed in a specific pathogen-free environment at four adults to a cage with corn cob bedding in Techniplast vent racks (Exton, PA, USA), and were kept on a 12 h light/dark cycle at $21 \pm 2°C$ with free access to reverse osmosis filtered water and food (Prolab 5P76 Isopro 3000; 5.4% fat by weight).

2.2 Contractile responses.

Gastric fundus smooth muscles were obtained by sharp dissection as described [21]. Each sheet of fundus smooth muscles was pinned out flat, cut into a rectangle of 10mm × 15mm, and then folded, in parallel with the circular muscles, into a rectangle of 10mm × 5mm. The ends were tied with surgical thread, and one end was attached to the tissue holder with a clip, and the other end attached to a Fort 10 isometric strain gauge (WPI, Sarasota, FL, USA) [14]. Each muscle strip was stretched to 1.6 times its initial length, and incubated for 30–45 min in 37°C oxygenated Krebs-Ringers Buffer (KRB), followed by an additional 30 min incubation in 0.3 μM tetrodotoxin prior to carbachol (CCh) addition, or 100μM L-NAME and 1μM MRS2500 prior to the delivery of square-wave pulses of electrical field stimulation (EFS) of 0.3 ms duration, 10Hz, 150 V, 5sec duration (supra-maximal voltage; Grass S48 stimulator). Contractile responses were acquired and analyzed using Acqknowledge 3.2.7 software (BIOPAC Systems, Santa Barbara, CA, USA). EFS or CCh treated tissues were collected at 5 sec and 1 min after stimulation, respectively. The myobath chamber was quickly lowered and the tissue was rapidly immersed into room temperature PBS containing 4% (w/v) paraformaldehyde (PFA). During EFS, the stimulation was on while lowering the bath and submerging the tissue into the 4% PFA. The muscles were fixed for 15 min, washed in PBS at room temperature for 3 times, and then stored at 4°C in PBS 0.1% sodium azide.

2.3 Immunofluorescence and isPLA.

Fixed gastric fundus smooth muscle strips were cryo-protected with PBS/30% sucrose at 4°C, embedded in OCT, and frozen at −80°C. The blocks were cut using a microtome into 10 μm transverse cross sections through the circular smooth muscle layer, and placed onto Vectabond (SP-1800) coated glass slides (Fisherbrand Superfrost Plus Microscope Slides, 12–550-15). After 20 min microwave heat-induced antigen retrieval in Tris-EDTA buffer (10 mM Tris base, 1 mM EDTA solution, 0.05% Tween 20, pH 9.0), the slides were

permeabilized and blocked with PBS containing 0.2% tween-20 and 1% bovine serum albumin for 10 min at room temperature. The slides were then incubated overnight at 4°C with the appropriate primary antibody as indicated below. Immunolabeling was performed with the appropriate Alexa-488 or Alexa-594 conjugated secondary antibody (Cell Signaling Technology, USA) against the primary antibody (1:500 for 30 min at room temperature in PBS. Finally, mounting medium containing DAPI was applied to the slides to label the nuclei.

For isPLA, gastric fundus smooth muscle tissue sections were treated with heat-induced antigen retrieval, then permeabilized and blocked with PBS containing 0.2% Tween-20 and 1% bovine serum albumin for 10 min at room temperature. PLA was performed according to the manufacturer's instructions using the Duolink *In Situ* Detection Reagents Red DUO92008 (Sigma-Aldrich, Olink Bioscience, Sweden). The muscle sections were incubated with each primary antibody (1:400 dilution) sequentially for 1 hour at room temperature. The slides were then incubated with the appropriate PLA probes (diluted 1:5 in PBS containing 0.05% Tween-20 and 3% bovine serum albumin) in a pre-heated humidified chamber at 37°C for 1h, followed by the ligation (30 minutes, 37 °C) and amplification (70 minutes, 37 °C) reactions. Finally, mounting medium with DAPI was used to label nuclei blue. It has been reported that the number of PLA signals generated can decrease as the kits get older [42]. We did not experience any differences in the PLA results as the kits aged. However, control and treated muscle sections were compared using Duolink Detection kits from the same lot number prior to the lot expiration date.

Antibodies: rabbit anti-β1integrin, GTX128839; mouse anti-talin, GTX11188; mouse anti-enteric γ-actin, GTX101794, GeneTex, Irvine, CA, USA. Mouse anti-LC20, sc-28329; rabbit anti-pS19, sc-12896; rabbit anti-talin, sc-15336; rabbit anti-MYPT1, sc-25618; rabbit anti-pT853, sc-17432-R; rabbit anti-pT696, sc-17556-R; mouse anti-CPI-17, sc-48406; rabbit anti-pT38, sc-17560; goat anti-β1integrin, sc-6622; mouse anti-α8integrin, sc-365798; mouse anti-PKC, sc-80; mouse anti-RhoA, sc-418; rabbit anti-ROCK2, sc-5561; rabbit anti-LC20, sc-15370, Santa Cruz Biotechnologies, Santa Cruz, CA, USA. Rabbit anti-pY397-FAK, #8556; rabbit anti-FAK, #3281; rabbit anti-Akt #4691, (Cell Signaling Technology, Danvers, MA, USA). Rabbit non-immune IgG, Sigma-Aldrich, St. Louis, MO, USA.

2.4   Confocal microscopy and image acquisition.

The slides were examined using an LSM510 Meta (Zeiss, Jena, Germany) or Fluoview FV1000 confocal microscope (Olympus, Center Valley, PA, USA). Confocal micrographs are digital composites of the Z-series of scans (1 μm optical sections of 10 μm thick sections). Settings were fixed at the beginning of both acquisition and analysis steps and were unchanged. Brightness and contrast were slightly adjusted after merging. Final images were constructed using FV10-ASW 2.1 software (Olympus, USA). As indicated, the number of PLA red spots per area was normalized to the number of PLA spots from LC20/LC20 PLA, using rabbit anti-LC20 (sc-15370; 1:400) and mouse anti-LC20 (sc-28329; 1:400) antibodies. Each image is representative of labeling experiments from 3 sections from 3 fundus muscles, and 2 images collected from each fundus muscle section. Scale bars, 10 μm.

2.5 Statistical analysis.

Fiji software was used to count PLA spots [41]. The red channel was digitally removed from the raw tiff image, and the threshold adjusted with the MaxEntropy thresholding algorithm [43]. The PLA spots were counted by particle analysis with the particle size set between 6 and 40 pixels. The normalized PLA spots counts were analyzed by parametric repeated tests of ANOVA using Prism 6.01 software, and are reported as the average ± SD. *T*-test was used to test the significance and P < 0.05 is considered significant. To measure the cross-sectional areas of cells, the smooth muscle tissue sections were immunolabeled with anti-β1integrin to outline the plasma membranes, and the cross-sectional area of each cell was calculated using Image J/Fiji software [41].

2.6 Drugs.

Tetrodotoxin and atropine were obtained from EMD Millipore, Billerica, MA, USA; Carbachol, L-NAME, and PF-431396 were obtained from Sigma-Aldrich, St. Louis, MO, USA; MRS2500 was purchased from Tocris Bioscience, Minneapolis, MN, USA.

3. RESULTS

3.1 Data validation for smooth muscle tissue PLA

To validate smooth muscle tissue PLA signals, we designed positive and negative biological controls based on the current experimental evidence and the molecular interaction database IntAct [44]. The direct interaction between γ-actin and smooth muscle LC20 is essential for smooth muscle cell contraction [45]. Talin physically links actin filaments to integrins by directly binding to γ-actin [46]. In other situations, PLA can detect two proteins within a multi-protein complex, that do not directly interact with each other, but are still in close proximity (<40nm) [47]. As a positive control for the use of tissue-PLA for proteins in the same protein complex but not directly interacting, we chose RhoA and MYPT1. In the IntAct database, RhoA and MYPT1 are identified as a co-complex interaction via ROCK2, instead of a direct interaction [44]. For a negative biological control, we examined the PLA signals generated from talin and Akt. Upon activation, talin translocates from the cytoplasm to integrins in focal adhesions, while Akt translocates from the cytoplasm to PIP3 in the plasma membrane [48] [46]. Talin and Akt do not interact according to the IntAct database.

As shown in Figure 1 each antibody used for the positive controls was validated by immunofluorescence. The separate γ-actin and LC20 immunofluorescence images show extensive distribution of γ-actin and LC20 throughout the cytoplasm of smooth muscle cells, as expected (Fig. 1A). Overlay of the γ-actin and LC20 images shows extensive co-localization of γ-actin and LC20 throughout the cytoplasm of smooth muscle cells, as expected (Fig. 1A). The γ-actin/LC20 PLA generated numerous signals as well (Fig. 1A). Figure 1B again shows extensive distribution of γ-actin throughout the cytoplasm, while the talin immunofluorescence shows punctate staining, as expected for a protein associated with integrins at the plasma membrane [49]. Overlay of the γ-actin and talin images shows that γ-actin and talin are co-localized at the plasma membrane, not throughout the cytoplasm (Fig. 1B). The γ-actin/talin PLA also generated numerous spots (Fig. 1B). The Rhoa and MYPT1 immuno-fluorescence images show extensive distribution of RhoA and MYPT1

throughout the cytoplasm of smooth muscle cells, and as expected, overlaying the RhoA and MYPT1 images shows extensive co-localization of RhoA and MYPT1 within the smooth muscle (Fig. 1C). RhoA/MYPT1 PLA also generated robust signals (Fig. 1C). Figure 1D shows that the antibodies used for the negative biological controls generated extensive immunofluorescence signals in the smooth muscles. Figure 1D shows punctate talin immunofluorescence staining at the plasma membrane, while the Akt immunofluorescence shows a more uniform Akt distribution. Overlay of the talin and Akt images shows very little co-localization of talin and Akt, and the talin/Akt PLA shows no detectable signals (Fig. 1D). Thus, the results of these positive and negative biological controls for isPLA validate the use of PLA for examining direct and indirect protein-protein interactions in smooth muscle tissues. Finally, we validated the PLA approach with negative technical controls. Virtually no PLA signals are detected when a non-immune IgG is paired with a specific antibody (Fig. 1E), or when only one specific antibody is present (Fig. 1F), or when both specific primary antibodies are omitted (Fig. 1G). These findings are consistent with the low false positive rates found with PLA [50].

3.2 PLA Thresholding and Spot Counting

The PLA spots visualized by fluorescence microscopy are typically expected to be around 1μm in diameter. [4]. Oversized PLA spots usually occur from oversaturated primary antibody, improper antibody dilutions, or insufficient washing, as shown in the α8integrin/β1integrin isPLA of a tissue section of gastric fundus smooth muscle in Fig. 2A [4]. Thus it is necessary to filter out the false-positive, improperly sized spots and set the parameters for counting true positive PLA spots. To count the PLA spots, we used Fiji to extract and convert the red channel to black and white (Fig. 2B), invert the black and white image (Fig. 2C), and set the pixel threshold using the MaxEntropy thresholding method, which helps the deconvolution of the PLA signals [43, 51]. Based on the PLA methodology, the 70 min rolling circle amplification reaction should generate PLA spot sizes between 1μm and 3μm in diameter [8]. Thus, we set the particle analysis to filter out spot sizes < 0.5μm and > 3μm (Fig. 2D). After spot thresholding, the skewed distribution of the PLA spot sizes before thresholding (Fig. 2E) are restored to a normal distribution (Fig. 2F), resulting in a less biased PLA spot count after these statistical corrections.

3.3 Internal controls for PLA spot quantitation in relaxed and contracted gastric fundus smooth muscles.

To compare the PLA signals from protein-protein interactions or protein phosphorylation in sections from contracted and resting (control) smooth muscles, we measured the force generated by isometric contractions. Isometric contractions generate force without a change in the length or morphometry of the muscle tissue [40, 52]. This ensures that the number of smooth muscle cells, and their cross sectional diameters, within the image area of unstimulated and unstimulated muscles, should be similar [53]. Since the cell density and cell size within the image area should be similar, the number of actin and myosin filaments within the image area would also be expected to be similar. The typical force generated by isometric contraction of fundus smooth muscle strips with 1μM CCh or 10Hz EFS is shown in Figure 3A and 3B. To measure the areas of the smooth muscle cells, cross-sections of unstimulated and contracted gastric fundus smooth muscles were labeled by β1integrin

immunofluorescent staining to obtain an outline of the plasma membrane, and the cross-sectional area of each cell was calculated using Image J/Fiji software [41]. The cross sections of cells in unstimulated gastric fundus smooth muscles (Fig. 3C), or muscles stimulated with 1 μM CCh (Fig. 3D), or 10Hz EFS (Fig. 3E) appear to be similar. Analysis of the cellular cross sectional areas from unstimulated gastric fundus smooth muscles, or muscles stimulated with 1μM CCh, or 10Hz EFS shows that the average cellular cross-sectional areas ± SD are not significantly different (Fig. 3I). We also performed single protein PLA of LC20 using primary antibodies from different host species against LC20 to quantify the PLA spots from smooth muscle myosin light chains, as an internal standard, and as an indirect measurement of smooth muscle cell density. In this study, we analyzed the PLA signals by imaging the same volume (same area and z-depth) of the smooth muscle tissue sections, and measuring the cross sectional area of the image. The average ± SD numbers of LC20/LC20 PLA spots in unstimulated gastric fundus smooth muscles (Fig. 3F), or muscles stimulated with 1μM CCh (Fig. 3G), or 10Hz EFS (Fig. 3H) are not significantly different.

3.4 Measuring MYPT1, CPI-17, and LC20 phosphorylation by isPLA in response to cholinergic stimulation

To assess the ability of isPLA to detect protein phosphorylation in smooth muscles, we examined the phosphorylation of the Ca^{2+} sensitization proteins CPI-17 and MYPT1, and LC20 phosphorylation, in response to bath applied CCh, or EFS of cholinergic motor neurons. Primary antibodies from different species were utilized to detect the target protein and the phosphorylated Ser or Thr amino acid residue. Stimulating fundus muscles with 1μM CCh for 1 min increased MYPT1 T853 phosphorylation 1.8 ± 0.1-fold, as indicated by the increased number of MYPT1/pT853 PLA spots (Fig. 4A, 4B). In contrast, EFS of cholinergic motor neurons for 5 sec did not significantly increase MYPT1 T853 phosphorylation (Fig. 4A, 4B). Figure 4C, and 4D shows that neither CCh or EFS increased MYPT1 T696 phosphorylation, consistent with our previous findings [15]. CPI-17 T38 phosphorylation was increased 1.6 ± 0.09-fold and 1.3 ± 0.05-fold in response to CCh or EFS stimulation, respectively (Fig. 4E, 4F). LC20 S19 phosphorylation was increased 1.8 ± 0.15-fold by CCh treatment, but was unchanged by EFS of cholinergic motor neurons (Fig. 4G, 4H). Basal levels of MYPT1, CPI-17, and LC20 phosphorylation were detected by isPLA (Control), and the changes in MYPT1, CPI-17, and LC20 phosphorylation are consistent with our previous western blot data [15].

3.5 Effects of cholinergic stimulation and the FAK inhibitor PF-431396 on β1integrin/FAK association.

We previously found that FAK is phosphorylated at the activation Y397, in response to EFS-evoked cholinergic contractions of murine gastric fundus muscles [21]. Since FAK Y397 phosphorylation is associated with the recruitment of FAK to integrins within focal adhesions [54], we used isPLA to examine the localization of FAK and β1integrin in response to EFS-evoked cholinergic contractions. As shown in Figure 5A and 5B there is a basal FAK/β1integrin interaction in resting muscles, which is significantly increased 3.1 ± 0.15-fold by 10Hz, 5sec EFS. In addition, PF-431396 blocked the EFS-evoked increase in FAK/β1integrin interaction (Fig. 5C, 5D). Along with the increase in the FAK/β1integrin

interaction, the amount of Y397 phosphorylated FAK associated with β1integrin increased by approximately 3-fold in response to EFS-evoked cholinergic contractions (Fig. 5C, 5D). No detectable FAK-pY397/β1integrin PLA signal was found in EFS stimulated smooth muscle pretreated with 0.3 μM PF-431396 (Fig 5C, 5D).

3.6 Effects of cholinergic stimulation and PF-431396 on β1integrin association with PKC and CPI-17.

We previously found that PF-431396 inhibits the increase in CPI-17 T38 phosphorylation during EFS-evoked cholinergic contractions [21]. Because FAK is recruited to β1integrin in focal adhesions, we examined whether CPI-17 is also recruited and phosphorylated at focal adhesions. As shown in Figure 6A and 6B, there is a basal CPI-17/β1integrin interaction in resting muscles, which is increased 2.4 ± 0.08-fold by 10Hz, 5sec EFS. In addition, PF-431396 blocked the EFS-evoked increase in FAK/β1integrin interaction (Fig. 6A, 6B). Along with the increase in the FAK/β1integrin interaction, the amount of T38 phosphorylated CPI-17 associated with β1integrin increased by 3.1 ± 0.04-fold in response to EFS-evoked cholinergic contractions (Fig. 5C, 5D). PF-431396 blocked the EFS-evoked increases in the CPI-17/β1integrin interaction (Fig. 5A, 5B), and the T38 phosphorylated CPI-17 associated with β1integrin (Fig. 5C, 5D). CPI-17 is phosphorylated by PKC activation in response to cholinergic stimulation in smooth muscle tissue [55–58]. Active PKC has been reported to accumulate near β1integrin in smooth muscle [59–61]. Since CPI-17 is phosphorylated by PKC, we examined whether PKC interacts with β1integrin in murine gastric fundus smooth muscles, using a pan-PKC antibody. Figure 6E and 6F show that there is a basal PKC/β1integrin interaction in resting muscles, that is increased 2.3 ± 0.3-fold by 10Hz, 5 sec EFS. In addition, PF-431396 blocked the EFS-evoked increase in the PKC/β1integrin interaction (Fig. 6E, 6F).

3.7 Effects of cholinergic stimulation and PF-431396 on the association of RhoA, ROCK2, MYPT1 with β1integrin.

The findings in Figure 4 showing that EFS does not increase MYPT1 T853 phosphorylation are consistent with our previous findings by western blot analyses [26]. However, previous reports show that ROCK2, RhoA, and MYPT1 are distributed between the cytosol and the membrane fractions of smooth muscles [62–64]. Thus, we examined the effects of EFS-evoked cholinergic motor neuron activation on the interactions between β1integrin and RhoA, ROCK2, and MYPT1. As shown in Figure 7A and 7B, there is a substantial basal level of RhoA/β1integrin interactions in resting muscles, which is increased 2.1 ± 0.3-fold by 10Hz, 5sec EFS. The EFS-evoked increase in RhoA/β1integrin interactions was prevented by PF-431396 (Fig. 7A, 7B). ROCK2/β1integrin interactions are low in resting muscles, but are increased 3.6 ± 0.15-fold by 10Hz, 5sec EFS (Fig. 7C, 7D). The EFS-evoked increase in ROCK2/β1integrin interactions was also prevented by PF-431396. In contrast, there are very few MYPT1/β1integrin and pT853/β1integrin interactions in resting muscles, and 10Hz 5 sec EFS either in the absence or presence of PF-431396 had no effect on these interactions (Fig. 7E, 7F).

3.8   Effects of cholinergic stimulation on the association of MYPT1 and phosphorylated MYPT1 with LC20.

The findings in Figures 4 and 7 showing that 10Hz 5sec EFS has no effect on MYPT1 T853 phosphorylation and the association of MYPT1 with β1integrin led us to examine the effects of cholinergic stimulation on the association of MYPT1 with LC20. As shown in Figure 8, there is a constitutive level of MYPT1 associated with LC20 in resting muscles, that was not affected by 10Hz 5sec EFS. In contrast, 1μM CCh stimulation reduced the association of MYPT1 with LC20 slightly over 2-fold.

3.9   Effects of cholinergic stimulation and PF-431396 on β1integrin association with LC20 and γ-actin.

The findings in Figure 4 showing that 10Hz 5sec EFS increased LC20 S19 phosphorylation are different from our previous findings by western blot analyses showing that EFS of gastric fundus smooth muscle strips does not increase S19 phosphorylation [26]. Thus, we examined whether LC20 is selectively phosphorylated in a distinct subcellular compartment of gastric fundus muscles, by examining the effects of EFS-evoked cholinergic motor neuron activation on the interactions between β1integrin, LC20, S19 phosphorylated LC20, and γ-actin. Figure 9A and 9B shows that there is a low basal level of LC20/β1integrin interactions in resting muscles, that is unaffected by 10Hz 5sec EFS in the absence or presence of PF-431396. In contrast, there is a lower level of S19 phosphorylated LC20 associated with β1integrin in resting muscles that is increased 2.4 ± 0.4-fold by 10Hz, 5 sec EFS. The EFS-evoked increase in S19 phosphorylated LC20 associated with β1integrin was prevented by PF-431396 (Fig. 9C, 9D). Consistent with the attachment of actin filaments to β1integrin at focal adhesions, the level of γ-actin/β1integrin interactions is high in gastric fundus smooth muscles (Fig. 9E, 9F). Interestingly, 10Hz 5 sec EFS decreased the γ-actin/β1integrin interactions by about 3-fold, while PF-431396 partially blocked the decrease in the γ-actin/β1integrin interactions by 10Hz 5sec EFS (Fig. 9E, 9F).

4.   Discussion

In this study, we optimized the use of in situ PLA in smooth muscle tissue sections in order to quantitatively compare protein phosphorylation data from resting muscles and isometrically contracted smooth muscles. We assessed LC20/LC20 single protein PLA and cellular cross-sectional areas as internal controls to quantify changes in PLA signals relative to either internal standard. We validated a set of positive and negative controls for direct protein-protein interactions, co-complex interactions, and PLA technical controls. We demonstrated the analysis steps to quantify PLA signal counts and eliminate noise. As required for the antibody-based PLA approach, we performed validation immunofluorescence immunohistochemistry to show that the primary antibodies each individually detect their intended target antigens. To validate smooth muscle tissue isPLA, we performed the following controls: γ-actin/LC20, γ-actin/talin, RhoA/MYPT1 and talin/Akt PLA for positive and negative biological controls, respectively. Positive and negative controls can be identified from published biochemical data and the IntAct protein-protein interaction database [44]. In smooth muscles, γ-actin and LC20 are in close proximity due to the binding of the myosin globular head to actin filaments, talin links actin

myofilaments to integrins, and RhoA is present in a multiprotein complex with MYPT1 [65]. Proteins that are located in different subcellular compartments or organelles are good negative controls. Akt translocates to the plasma membrane, by the binding of its PH domains to PIP3, and is not in close proximity to talin which is located at focal adhesions [66]. In order to generate quantifiable PLA data, saturation of the PLA signal should be avoided by using the proper primary antibody concentrations [4]. We carried out primary antibody titrations to adjust the PLA spot size and density. We used the MaxEntropy algorithm to adjust the thresholding parameters between 0.5μm and 3μm size to filter out outliers/artifacts and to make sure the PLA spot size distribution is close to a normal distribution [43] (Fig. 3). Finally, we used PLA spot quantitation with Fiji (Fig. 2E, 2F) to remove PLA noise and avoid the time consuming and prone-to-bias quantitation process by manual and/or ordinal scoring quantitation [67, 68].

In addition, similar to the notion of using a "housekeeping" protein as the internal control for traditional western blot quantitation, we developed internal controls for isPLA spot quantitation. Typically, PLA signals are quantified relative to the number of cell nuclei, or the total PLA signal intensity [35]. However, quantifying PLA signals relative to the number of nuclei is not possible in a tissue section because the slice may not bisect every nucleus of every cell in the section. We considered quantifying PLA signals relative to the cell number, but in situ PLA of muscle tissue sections posed an additional variable to consider when analyzing changes in the amounts of phosphorylated proteins or protein-protein interactions by spot counts, where each spot represents a discrete phospo-protein or a protein-protein interaction; namely, the apparent changes in spot abundance due to the movement of spots into, or out of a given area of the tissue section due to prior changes in the length and width of the muscle tissue as it shortens and contracts. In an isometric contraction, the muscle contracts and generates force, but does not shorten and change its length [69, 70]. Measuring the force generated by muscle strips stimulated to undergo isometric contractions avoids morphological changes to the smooth muscle cells. Thus, the lengths and cross-sectional diameters, of individual smooth muscle cells should not significantly change, nor should the positions of intracellular proteins change, unless protein translocation mechanisms are activated in response to the contractile stimulus. In order to quantitate PLA spots relative to the cell cross-sectional area, we used immunofluorescence staining of β1integrin to label cell membranes, and measured the diameters, and numbers of the smooth muscle cells in in cross sections of tissue slices. Using the cell diameters, we used ImageJ to calculate the cross-sectional areas of smooth muscle cells from unstimulated muscles, and from muscles isometrically contracted by EFS of cholinergic motor neurons, or by CCh treatment. The results in Figure 3 indicate that the morphology and density of the smooth muscle cells in uncontracted and isometrically contracted fundus smooth muscles are similar. These findings suggested that the density of LC20 should be similar, and that LC20 single protein PLA would generate similar numbers of spots from uncontracted, and isometrically contracted smooth muscles that could be used as an additional internal standard for measuring changes in protein phosphorylation or protein-protein interactions. Similar to the cross-sectional areas, we found that the numbers of LC20 single protein PLA spots were also similar from uncontracted and isometrically contracted fundus smooth muscles. Together, these findings indicate that the cross-sectional areas of the smooth muscle cells or

LC20/LC20 PLA spot counts can be used as internal standards for comparing different experimental groups, when the muscles are set up for isometric contractions in response to contractile agonists. This approach may not be applicable to smooth muscles undergoing isotonic contractions, in which the muscle length does change. As smooth muscles shorten during isotonic contractions, an dynamic process called length adaptation occurs, which involves structural rearrangements of the cytoskeleton and contractile myofilaments to maximize overlap between the thick and thin myosin and actin filaments [22, 71, 72]. The interconversion of myosin between monomeric, oligomeric and filamentous myosin occurs during length adaptation, allowing smooth muscles to function and generate force over a much broader length range than striated muscle [71]. In addition, the cross sectional areas of the smooth muscle cells increase and their packing density decreases [73]. The cross sectional areas increase in proportion to the decrease in length, suggesting that the ends of the muscle cells are pulled in towards the middle portions of the cells, as each muscle cell shortens [73]. These changes in cell morphology and in the numbers and distribution of contractile myofilaments make it difficult to use this is PLA approach to compare relative and absolute changes in protein-protein interactions and protein phosphorylation between relaxed and isotonically contracted smooth muscles.

Using isometrically contracted smooth muscle strips, we found increased MYPT1, CPI-17, and LC20 phosphorylation in response to CCh treatment of gastric fundus smooth muscles by pT853/MYPT1, pT38/CPI-17 PLA, and pS19/LC20 PLA. In addition, we found that EFS did not significantly increase the pT853/MYPT1 PLA spot count. These findings agree with the data from our previous studies obtained by SDS-PAGE and western blotting analyses [15]. We initially utilized the PLA approach because of the observed lack of increased MYPT1 T853 phosphorylation, as measured by SDS-PAGE and western blotting analysis, in response to cholinergic motor neuron stimulation [15]. We thought that SDS-PAGE and western blot analysis of whole muscle tissue homogenates might not be sensitive enough to detect an increase in MYPT1 phosphorylation occurring preferentially in a subcellular compartment. Due to the preservation of cellular and subcellular structures, in situ PLA of muscle tissue sections provides spatial information regarding MYPT1 phosphorylation, and could possibly detect changes in compartmentalized MYPT1 phosphorylation. However, the isPLA analyses showed that CCh treatment, but not EFS, significantly increased the pT853/MYPT1 PLA spot count. These findings are consistent with other studies showing that MYPT1 phosphorylation is increased by pharmacological stimulation via exogenously added cholinergic agonists, but not by physiological stimulation of cholinergic neurotransmission [74, 75].

We used in situ PLA to further analyze our previous findings showing that FAK activation plays an important role in the contractile response of gastric fundus muscles to cholinergic stimulation [21]. We measured the increase in Y397 phosphorylation by Wes analysis as an indicator of FAK activation evoked by CCh or by EFS-evoked cholinergic motor neuron stimulation. However, since the effector functions of FAK require its association with integrins, we used in situ PLA to extend these findings to demonstrate that upon activation by Y397 phosphorylation, FAK also associates with β1integrin. As shown in Figure 5, EFS of gastric fundus muscles increased the association of FAK, and Y397 phosphorylated FAK, with β1integrin, and this interaction is sensitive to the FAK inhibitor PF431396. These

findings are consistent with previous findings that the increase in FAK association with β1 integrin is due to increased association of Y397 phosphorylated FAK with β1integrin [16, 76–79].

We also previously found that the EFS-evoked CPI-17 T38 phosphorylation by PKC is inhibited by FAK inhibition [21]. These findings suggested that FAK is an upstream regulator of PKC activation by cholinergic motor neuron stimulation. Using an antibody specific for PKC α, and β, Figure 6 shows that EFS of gastric fundus muscles increased the association of α/βPKC with β1integrin. Since the activation of α/βPKC involves translocation to the plasma membrane [80], these findings suggest that FAK regulation of α/βPKC activity may occur at β1integrins. The association of CPI-17 and T38 phosphorylated CPI-17 with β1integrin was also increased by EFS of gastric fundus muscles, and these interactions are sensitive to the FAK inhibitor PF431396. These findings are consistent with the inhibition of EFS-evoked CPI-17 T38 phosphorylation by PKC by FAK inhibition.

We found significant increases in the association of RhoA and ROCK2 with β1integrin in response to EFS, and these EFS-evoked increases in RhoA and ROCK2/β1integrin interactions were prevented by PF-431396 (Fig. 7A, 7B), suggesting that FAK activation is involved in the EVS-evoked increase in the association of RhoA and ROCK2 with β1integrin. It is known that activation and translocation of the RhoA GEF Rgnef to focal adhesions is dependent upon FAK activation [81]. Thus, FAK inhibition in gastric antrum smooth muscles with PF-431396 may disrupt RhoA activation by interfering with RhoA GEF activation, and subsequently reduce the binding of GTP-RhoA to ROCK2. The isPLA results show very few MYPT1/β1integrin and pT853/β1integrin interactions in resting muscles, and 10Hz 5sec EFS either in the absence or presence of PF-431396 had no effect on these interactions. These findings suggest that association with focal adhesions is not important for the regulation of MLCP activity by MYPT1 T853 phosphorylation, and that the EFS-evoked increased association of RhoA and ROCK2 with β1integrin may be involved in other effector functions of RhoA and ROCK2 that are important for the cytoskeletal remodeling at focal adhesion-actin filament attachments that occurs during contractile responses [82–84]. The role of MYPT1 T853 phosphorylation in regulating MLCP activity and LC20 S19 phosphorylation is still unresolved. In contrast, it is known that the phosphorylated T696 residue directly docks at the active site of PP1, causing autoinhibition and decreased MLCP activity towards the phosphorylated S19 of LC20 [85, 86]. The level of constitutively phosphorylated T696 is high in resting smooth muscle tissues and is thought to confer constitutive inhibition of MLCP [75, 85]. However, most reports show that MYPT1 T696 phosphorylation is unchanged in response to ROCK2 activation by contractile stimuli [9, 15, 56]. Previous studies showed that T853 phosphorylation induces the dissociation of MLCP from myosin, supporting ROCK2-MYPT1-mediated MLCP inhibition leading to increased LC20 S19 phosphorylation [85, 87]. Our finding in Figure 4 showing that CCh stimulation, but not EFS, increased MYPT1 T853 phosphorylation, and our finding in Figure 8 showing that CCh stimulation, but not EFS, decreased the association of MYPT1 with LC20 are consistent with T853 phosphorylation inducing the dissociation of MLCP from myosin. More recent studies show that although MYPT1 T853 phosphorylation is elevated in response to ROCK activation, it has little to no effect on MLCP activity [74, 75]. However, ROCK2 inhibition blocks the agonist-induced Ca^{2+} sensitization of smooth

muscle, suggesting that ROCK2 activity is necessary for smooth muscle Ca^{2+} sensitization [15, 74].

The findings in Figure 4 showing that 10Hz 5sec EFS increased LC20 S19 phosphorylation are different from our previous findings by western blot analyses showing that EFS of gastric fundus smooth muscle strips does not increase S19 phosphorylation [15]. The tension generated by actin-myosin cross-bridge formation is transmitted to the ECM at focal adhesions (23). Since spatial information is provided by isPLA, we examined whether LC20 is selectively phosphorylated in a distinct subcellular compartment of gastric fundus muscles. Figures 9A and 9B show that there is a basal level of LC20/ β1integrin interactions in resting muscles, that is unaffected by 10Hz 5sec EFS in the absence or presence of PF-431396. In contrast, there is a lower level of S19 phosphorylated LC20 associated with β1integrin in resting muscles that is increased about 2–3-fold by 10Hz, 5sec EFS, suggesting that the EFS-evoked contraction increases the phosphorylation of existing LC20 at focal adhesions. These results are consistent with the function of myofilaments to transmit force through focal adhesions to the extracellular matrix. The EFS-evoked increase in S19 phosphorylated LC20 associated with β1integrin was prevented by PF-431396 (Fig. 9C, 9D), suggesting that the interaction of FAK with β1integrin is required. It is increasingly evident that in order to transmit force, the sliding actomyosin filaments must be anchored to the opposing sides of a smooth muscle cell, as well as to other smooth muscle cells via the extra cellular matrix (ECM). This anchoring process occurs as part of a dynamic, stimulus-driven cortical cytoskeletal reorganization and actin polymerization at membrane focal adhesions [23]. The use of isPLA to examine the cytoskeletal reorganization occurring at focal adhesions during contractile responses may lead to a better understanding of the spatiotemporal aspects of the process of myofilament linkage and attachment to focal adhesion complexes. For example, consistent with the attachment of actin filaments to β1integrin at focal adhesions for force transmission to the extracellular matrix, we found that the level of γ-actin/β1integrin interactions is high in gastric fundus smooth muscles (Fig. 8E, 8F). Interestingly, 10Hz 5sec EFS decreased the γ-actin/β1integrin interactions by about 4-fold, while PF-431396 partially blocked the decrease in the γ-actin/β1integrin interactions by 10Hz 5sec EFS (Fig. 8E, 8F). The attachment of actin myofilaments to β1integrin is mediated by talin [88–90]. Talin interacts directly with the cytoplasmic domain of β1integrin and actin filaments [91, 92]. The connection between β1integrins and myofilaments is further strengthened by vinculin binding to talin [76]. The length of the talin protein increases from less than 50 nm to as much as 350–400 nm as it is activated by binding to β1integrin [93]. Since proteins that are greater than 40 nm from each other are not detected by PLA, the decrease in actin/ β1integrin interactions we observed with the EFS-evoked contraction may be due to increased talin activation. Further studies are necessary to further investigate the mechanisms by which actin myofilaments attach to β1integrins and their role in force transmission.

In summary, we addressed several technical challenges associated with the analysis of smooth muscle tissue contractile responses by isPLA, and validated the isPLA approach for the analysis of protein phosphorylation and protein-protein interactions in contracting smooth muscles. With quantifiable isPLA data based on the cellular cross-sectional area or the LC20/LC20 PLA internal controls, noise filtering, and Fiji software spot quantitation, we

are able to use isPLA to detect changes in protein phosphorylation, protein-protein interactions, and protein complex composition during smooth muscle contractile responses. These smooth muscle tissue isPLA internal control and quantitation procedures are suitable not only for use in smooth muscles, but could also be applied to other tissue types characterized by dynamic functional responses. We anticipate that smooth muscle tissue isPLA will complement current experimental and computational approaches to enable quantifiable and in-depth smooth muscle tissue-level signaling studies.

Acknowledgements

Abbreviations

CCh	carbachol
Co-IP	co-immunoprecipitation
CPI-17	protein kinase C-potentiated inhibitor protein of 17 kDa (protein phosphatase 1 regulatory subunit 14A)
pT38	phosphorylated Thr38 of CPI-17
EFS	electrical field stimulation
FAK	focal adhesion kinase
isPLA	in situ proximity ligation assay
LC20	20 kDa myosin light chain (myosin regulatory light polypeptide 9)
pS19	phosphorylated Ser19 of LC20
MYLK	myosin light chain kinase, smooth muscle
MLCP	myosin light chain phosphatase
MYPT1	myosin phosphatase-targeting subunit 1, (protein phosphatase 1 regulatory subunit 12A)
pT853	phosphorylated Thr853 of MYPT1
pT696	phosphorylated Thr696 of MYPT1
PFA	paraformaldehyde
PKC	protein kinase C
Pyk2	protein tyrosine kinase 2β
ROCK2	Rho-associated protein kinase 2

References

[1]. Goel R, Harsha HC, Pandey A, Prasad TSK Human protein reference database and human proteinpedia as resources for phosphoproteome analysis. Mol. Biosystems. 8 (2012) 453–463. 10.1039/C1MB05340J

[2]. Ke M, Shen H, Wang L, Luo S, Lin L, Yang J, Tian R Identification, quantification, and site localization of protein posttranslational modifications via mass spectrometry-based proteomics. In: Mirzaei H, Carrasco M, editors. Modern Proteomics – sample preparation, analysis and practical applications. Springer International Publishing. (2016) 345–382. 10.1007/978-3-319-41448-5_17

[3]. Humphrey SJ, James DE, Mann M Protein phosphorylation: A major switch mechanism for metabolic regulation. Trends Endocrinol. Metabol. 26 (2015) 676–687. doi: 10.1016/j.tem. 2015.09.013.

[4]. Raykova D, Koos B, Asplund A, Gelléri M, Ivarsson Y, Danielson UH, Söderberg O Let there be light! Proteomes. 4 (2016) 36 10.3390/proteomes4040036

[5]. Weibrecht I, Leuchowius KJ, Clausson CM, Conze T, Jarvius M, Howell WM, Kamali-Moghaddam M, Soderberg O Proximity ligation assays: A recent addition to the proteomics toolbox. Exp. Rev. Proteomics. 7 (2010) 401–409. 10.1586/epr.10.10

[6]. Feist P, Hummon AB Proteomic challenges: Sample preparation techniques for microgram-quantity protein analysis from biological samples. Int. J. Mol. Sci. 16 (2015) 3537–3563. 10.3390/ijms16023537 [PubMed: 25664860]

[7]. Huber LA, Pfaller K, Vietor I Organelle proteomics: Implications for subcellular fractionation in proteomics. Circ. Res. 92 (2003) 962–968. 10.1161/01.RES.0000071748.48338.25 [PubMed: 12750306]

[8]. Söderberg O, Leuchowius K-J, Gullberg M, Jarvius M, Weibrecht I, Larsson L-G, Landegren U Characterizing proteins and their interactions in cells and tissues using the in situ proximity ligation assay. Methods. 45 (2008) 227–32. 10.1016/j.ymeth.2008.06.014 [PubMed: 18620061]

[9]. Gao N, Huang J, He W, Zhu M, Kamm KE, Stull JT Signaling through myosin light chain kinase in smooth muscles. J. Biol. Chem. 288 (2013) 7596–7605. 10.1074/jbc.M112.427112 [PubMed: 23362260]

[10]. Perrino BA Calcium sensitization mechanisms in gastrointestinal smooth muscles. J. Neurogastroenterol. Motil. 22 (2015) 213–225. 10.5056/jnm15186

[11]. Somlyo AP, Somlyo AV Ca^{2+} sensitivity of smooth muscle and nonmuscle myosin II: Modulated by G proteins, kinases, and myosin phosphatase. Physiol. Rev. 83 (2003) 1325–1358. 10.1152/physrev.00023.2003 [PubMed: 14506307]

[12]. Ding HL, Ryder JW, Stull JT, Kamm KE Signaling processes for initiating smooth muscle contraction upon neural stimulation. J. Biol. Chem. 284 (2009) 15541–15548. 10.1074/jbc.M900888200 [PubMed: 19349274]

[13]. Matsumura F, Hartshorne DJ Myosin phosphatase target subunit: Many roles in cell function. Biochem. Biophys. Res. Comm. 369 (2008) 149–156. 10.1016/j.bbrc.2007.12.090 [PubMed: 18155661]

[14]. Bhetwal BP, An CL, Fisher SA, Perrino BA Regulation of basal LC20 phosphorylation by MYPT11 and CPI-17 in murine gastric antrum, gastric fundus, and proximal colon smooth muscles. Neurogastroenterol. Motil. 23 (2011) e425–e436. 10.1111/j.1365-2982.2011.01769.x [PubMed: 21883701]

[15]. Bhetwal BP, Sanders KM, An C, Trappanese DM, Moreland RS, Perrino BA Ca^{2+} sensitization pathways accessed by cholinergic neurotransmission in the murine gastric fundus. J. Physiol. 591(Pt 12) (2013) 2971–2986. 10.1113/jphysiol.2013.255745 [PubMed: 23613531]

[16]. Kunit T, Gratzke C, Schreiber A, Strittmatter F, Waidelich R, Rutz B, Loidl W, Andersson K-E, Stief CG, Hennenberg M Inhibition of smooth muscle force generation by focal adhesion kinase inhibitors in the hyperplastic human prostate. Am. J. Physiol - Renal Physiol. 307 (2014) F823–F832. doi:10.1152/ajprenal.00011.2014. [PubMed: 25056351]

[17]. Mehta D, Gunst SJ Actin polymerization stimulated by contractile activation regulates force development in canine tracheal smooth muscle. J. Physiol. 519 (1999) 829–840. 10.1111/j. 14697793.1999.0829n.x [PubMed: 10457094]

[18]. Mills R, Mita M, Walsh M A role for the Ca^{2+}-dependent tyrosine kinase Pyk2 in tonic depolarization-induced vascular smooth muscle contraction. J. Muscle Res. Cell Motil. (2015) 1– 11. 10.1007/s10974-015-9416-2 [PubMed: 25452123]

[19]. Chen HC, Appeddu PA, Isoda H, Guan JL Phosphorylation of Tyrosine 397 in focal adhesion kinase is required for binding phosphatidylinositol 3-kinase. J. Biol. Chem. 271 (1996) 26329– 26334. 10.1074/jbc.271.42.26329 [PubMed: 8824286]

[20]. Mills RD, Mita M, Nakagawa J.i., Shoji M, Sutherland C, Walsh MP A role for the tyrosine kinase Pyk2 in depolarization-induced contraction of vascular smooth muscle. J Biol Chem. 290 (2015) 8677–8692. 10.1074/jbc.M114.633107 [PubMed: 25713079]

[21]. Xie Y, Han KH, Grainger N, Li W, Corrigan RD, Perrino BA A role for focal adhesion kinase in facilitating the contractile responses of murine gastric fundus smooth muscles. J. Physiol. 596 (2018) 2131–2146. 10.1113/JP275406 [PubMed: 29528115]

[22]. Gunst SJ, Tang DD, Opazo Saez A Cytoskeletal remodeling of the airway smooth muscle cell: A mechanism for adaptation to mechanical forces in the lung. Respir. Physiol. Neurobiol. 137 (2003) 151–68. 10.1016/S1569-9048(03)00144-7 [PubMed: 14516723]

[23]. Gunst SJ, Actin WZ cytoskeletal dynamics in smooth muscle: A new paradigm for the regulation of smooth muscle contraction. Am. J. Physiol. Cell Physiol. 295 (2008) C576–C587. 10.1152/ ajpcell.00253.2008 [PubMed: 18596210]

[24]. Lessey EC, Guilluy C, Burridge K From mechanical force to rhoa activation. Biochemistry 51 (2012) 7420–7432.10.1021/bi300758e [PubMed: 22931484]

[25]. Morgan KG The importance of the smooth muscle cytoskeleton to preterm labour. Exp Physiol. 99 (2014) 525–529. 10.1113/expphysiol.2013.072876 [PubMed: 24121284]

[26]. Bhetwal BP, An C, Baker SA, Lyon KL, Perrino BA Impaired contractile responses and altered expression and phosphorylation of Ca^{2+} sensitization proteins in gastric antrum smooth muscles from ob/ob mice. J. Muscle Res. Cell Motil. 34 (2013) 137–149. 10.1007/s10974-013-9341-1 [PubMed: 23576331]

[27]. Chakder S, Sarma DNK, Rattan S Mechanism of internal anal sphincter smooth muscle relaxation by phorbol 12,13-dibutyrate. Am. J. Physiol. - Gastrointest. Liver Physiol. 280 (2001) G1341–G1350. 10.1152/ajpgi.2001.280.6.G1341 [PubMed: 11352829]

[28]. Godoy MAF, Rattan S Role of rho kinase in the functional and dysfunctional tonic smooth muscles. Trends Pharmacol. Sci. 32 (2011) 384–393. 10.1016/j.tips.2011.03.005 [PubMed: 21497405]

[29]. Rattan S, Phillips BR, Maxwell PJ Rhoa/rho-kinase: Pathophysiologic and therapeutic implications in gastrointestinal smooth muscle tone and relaxation. Gastroenterol. 138 (2010) 13–18. doi: S0016-5085(09) 02033-2 [pii];10.1053/j.gastro.2009.11.016 [doi].

[30]. Kim SM, Kwon MS, Park CS, Choi KR, Chun JS, Ahn J, Song WK Modulation of Thr phosphorylation of integrin beta1 during muscle differentiation. J Biol Chem. 279 (2004) 7082– 7090. doi: 10.1074/jbc.M311581200. [PubMed: 14660602]

[31]. Smith PG, Garcia R, Kogerman L Mechanical strain increases protein tyrosine phosphorylation in airway smooth muscle cells. Exp Cell Res. 239 (1998) 353–360. 10.1006/excr.1997.3905 [PubMed: 9521853]

[32]. Wu Y, Huang Y, Herring BP, Gunst SJ Integrin-linked kinase regulates smooth muscle differentiation marker gene expression in airway tissue. Am. J. Physiol. - Lung Cellular Molec. Physiol. 295 (2008) L988–L997. 10.1152/ajplung.90202.2008 [PubMed: 18805960]

[33]. Zhang W, Huang Y, Gunst SJ P21-activated kinase (pak) regulates airway smooth muscle contraction by regulating paxillin complexes that mediate actin polymerization. J. Physiol. 594 (2016) 4879–4900. 10.1113/JP272132 [PubMed: 27038336]

[34]. Zhang W, Wu Y, Wu C, Gunst SJ Integrin-linked kinase regulates n-wasp-mediated actin polymerization and tension development in tracheal smooth muscle. J. Biol. Chem. 282 (2007) 34568–34580. 10.1074/jbc [PubMed: 17897939]

[35]. Jarvius M, Paulsson J, Weibrecht I, Leuchowius KJ, Andersson AC, Wahlby C, Gullberg M, Botling J, Sjoblom T, Markova B, Ostman A, Landegren U, Soderberg O In situ detection of phosphorylated platelet-derived growth factor receptor beta using a generalized proximity ligation method. Mol. Cell. Proteomics. 6 (2007) 1500–1509. 10.1074/mcp.M700166-MCP200 [PubMed: 17565975]

[36]. Blokzijl A, Friedman M, Ponten F, Landegren U Profiling protein expression and interactions: Proximity ligation as a tool for personalized medicine. J. Intern. Med. 268 (2010) 232–245. 10.1111/j.1365-2796.2010.02256.x [PubMed: 20695973]

[37]. Jung J, Lifland AW, Zurla C, Alonas EJ, Santangelo PJ Quantifying RNA-protein interactions in situ using modified-MTRIPS and proximity ligation. Nuc. Acid. Res. 41 (2013) e12 10.1093/nar/gks837

[38]. Law AMK, Yin JXM, Castillo L, Young AIJ, Piggin C, Rogers S, Caldon CE, Burgess A, Millar EKA, O'Toole SA, Gallego-Ortega D, Ormandy CJ, Oakes SR Andy's algorithms: New automated digital image analysis pipelines for Fiji. Sci Rep. 7 (2017) 15717 10.1038/s41598-017-15885-6 [PubMed: 29146920]

[39]. Mocanu M-M, Váradi T, Szöll si J, Nagy P Comparative analysis of fluorescence resonance energy transfer (FRET) and proximity ligation assay (PLA). Proteomics. 11 (2011) 2063–2070. doi: doi:10.1002/pmic.201100028. [PubMed: 21480528]

[40]. Fay FS, Delise CM Contraction of isolated smooth-muscle cells--structural changes. Proc. Natl. Acad. Sci U. S. A. 70 (1973) 641–645. 10.1073/pnas.70.3.641 [PubMed: 4197624]

[41]. Schindelin J, Arganda-Carreras I, Frise E, Kaynig V, Longair M, Pietzsch T, Preibisch S, Rueden C, Saalfeld S, Schmid B, Tinevez JY, White DJ, Hartenstein V, Eliceiri K, Tomancak P, Cardona A Fiji: An open-source platform for biological-image analysis. Nat. Meth. 9 (2012) 676–682. 10.1038/nmeth.2019

[42]. Ulke-Lemee A, Turner SR, MacDonald JA In situ analysis of smoothelin-like 1 and calmodulin interactions in smooth muscle cells by proximity ligation. J Cell Biochem. 116 (2015) 2667–2775. Epub 2015/04/30. doi: 10.1002/jcb.25215. [PubMed: 25923522]

[43]. Kapur J, Sahoo P, Wong A A new method for gray-level picture thresholding using the entropy of the histogram. Comput. Vis. Graph. Image. Process. 29 (1985) 273–285. 10.1016/0734-189X(85)90125-2

[44]. Orchard S, Ammari M, Aranda B, Breuza L, Briganti L, Broackes-Carter F, Campbell NH, Chavali G, Chen C, del-Toro N, Duesbury M, Dumousseau M, Galeota E, Hinz U, Iannuccelli M, Jagannathan S, Jimenez R, Khadake J, Lagreid A, Licata L, Lovering RC, Meldal B, Melidoni AN, Milagros M, Peluso D, Perfetto L, Porras P, Raghunath A, Ricard-Blum S, Roechert B, Stutz A, Tognolli M, van Roey K,Cesareni G, Hermjakob H The mintact project--Intact as a common curation platform for 11 molecular interaction databases. Nuc. Acid. Res. 42 (2014) D358–363. 10.1093/nar/gkt1115

[45]. Szent-Gyorgyi AG The role of actin-myosin interaction in contraction. Symp. Soc. Exp. Biol. 22 (1968) 17–42. [PubMed: 4235532]

[46]. Calderwood DA, Ginsberg MH Talin forges the links between integrins and actin. Nat. Cell Biol. 5 (2003) 694–697. 10.1038/ncb0803-694 [PubMed: 12894175]

[47]. Soderberg O, Gullberg M, Jarvius M, Ridderstrale K, Leuchowius KJ, Jarvius J, Wester K, Hydbring P, Bahram F, Larsson LG, Landegren U Direct observation of individual endogenous protein complexes in situ by proximity ligation. Nat. Meth. 3 (2006) 995–1000. 10.1038/nmeth947

[48]. Jo H, Lo P-K, Li Y, Loison F, Green S, Wang J, Silberstein LE, Ye K, Chen H, Luo HR Deactivation of Akt by a small molecule inhibitor targeting pleckstrin homology domain and facilitating Akt ubiquitination. Proc. Natl. Acad. Sci. U.S.A. 108 (2011) 6486–6491. 10.1073/pnas.1019062108 [PubMed: 21464312]

[49]. Szabo E, Papp S, Opas M Calreticulin and cell-substratum adhesion. Ca2+ Bind. Prot. 1 (2006) 86–91.

[50]. Greenwood C, Ruff D, Kirvell S, Johnson G, Dhillon HS, Bustin SA Proximity assays for sensitive quantification of proteins. Biomolec. Detect. Quant. 4 (2015) 10–16. 10.1016/j.bdq.2015.04.002

[51]. Di Gioia SA, Farinelli P, Letteboer SJ, Arsenijevic Y, Sharon D, Roepman R, Rivolta C Interactome analysis reveals that fam161a, deficient in recessive retinitis pigmentosa, is a component of the golgi-centrosomal network. Hum. Mol. Gen. 24 (2015) 3359–3371. 10.1093/hmg/ddv085 [PubMed: 25749990]

[52]. Stephens NL, Van Niekerk W Isometric and isotonic contractions in airway smooth muscle. Can. J. Physiol. Pharmacol. 55 (1977) 833–838. 10.1139/y77-112 [PubMed: 902157]

[53]. Tsukita S, Tsukita S, Usukura J, Ishikawa H Myosin filaments in smooth muscle cells of the guinea pig taenia coli: A freeze-substitution study. Eur. J. Cell Biol. 28 (1982) 195–201. [PubMed: 6890899]

[54]. Parsons JT Focal adhesion kinase: The first ten years. J. Cell Sci. 116 (2003) 1409–1416. 10.1242/jcs.00373 [PubMed: 12640026]

[55]. Kitazawa T, Eto M, Woodsome TP, Brautigan DL Agonists trigger G protein-mediated activation of the CPI-17 inhibitor phosphoprotein of myosin light chain phosphatase to enhance vascular smooth muscle contractility. J. Biol. Chem. 275 (2000) 9897–9900. 10.1074/jbc.275.14.9897 [PubMed: 10744661]

[56]. Kitazawa T, Eto M, Woodsome TP, Khalequzzaman M Phosphorylation of the myosin phosphatase targeting subunit and CPI-17 during Ca^{2+} sensitization in rabbit smooth muscle. J. Physiol. 546 (2003) 879–889. 10.1113/jphysiol.2002.029306 [PubMed: 12563012]

[57]. Zemlickova E, Johannes FJ, Aitken A, Dubois T Association of CPI-17 with protein kinase C and casein kinase I. Biochem. Biophys. Res. Commu. 316 (2004) 39–47. 10.1016/j.bbrc.2004.02.014

[58]. Wang T, Kendig DM, Trappanese DM, Smolock EM, Moreland RS Phorbol 12, 13-dibutyrate-induced, protein kinase C-mediated contraction of rabbit bladder smooth muscle. Front. Pharmacol. 2 (2012) 83 10.3389/fphar.2011.00083 [PubMed: 22232602]

[59]. Haller H, Lindschau C, Maasch C, Olthoff H, Kurscheid D, Luft FC Integrin-induced protein kinase calpha and cepsilon translocation to focal adhesions mediates vascular smooth muscle cell spreading. Circ Res. 82 (1998) 157–165. 10.1161/01.RES.82.2.157 [PubMed: 9468186]

[60]. Lanning NJ, Su HW, Argetsinger LS, Carter-Su C Identification of sh2b1beta as a focal adhesion protein that regulates focal adhesion size and number. J. Cell Sci. 124 (2011) 3095–3105. 10.1242/jcs.081547 [PubMed: 21878491]

[61]. Preston A, Haynes JM Alpha 1-adrenoceptor effects mediated by protein kinase C alpha in human cultured prostatic stromal cells. Br. J. Pharmacol. 138 (2003) 218–224. 10.1038/sj.bjp. 0705021 [PubMed: 12522093]

[62]. MacDonald JA, Borman MA, Murínyi A, Somlyo AV, Hartshorne DJ, Haystead TAJ Identification of the endogenous smooth muscle myosin phosphatase-associated kinase. Proc. Natl. Acad. Sci. U.S.A. 98 (2001) 2419–2424. 10.1073/pnas.041331498 [PubMed: 11226254]

[63]. Patel CA, Rattan S Cellular regulation of basal tone in internal anal sphincter smooth muscle by Rhoa/Rock. Am. J. Physiol. - Gastrointest. Liver Physiol. 292 (2007) G1747–G1756. 10.1152/ajpgi.00438.2006 [PubMed: 17379756]

[64]. Qi F, Ogawa K, Tokinaga Y, Uematsu N, Minonishi T, Hatano Y Volatile anesthetics inhibit angiotensin II-induced vascular contraction by modulating myosin light chain phosphatase inhibiting protein, CPI-17 and regulatory subunit, MYPT1 phosphorylation. Anesth Analg. 109 (2009) 412–417. doi:10.1213/ane.0b013e3181ac6d96 [PubMed: 19608811]

[65]. Surks HK, Richards CT, Mendelsohn ME Myosin phosphatase-Rho interacting protein. A new member of the myosin phosphatase complex that directly binds Rhoa. J Biol Chem. 278 (2003) 51484–51493. doi: 10.1074/jbc.M305622200.P [PubMed: 14506264]

[66]. Liao Y, Hung MC Physiological regulation of Akt activity and stability. Am.J. Tanslat. Res. 2 (2010) 19–42.

[67]. Allalou A, Wahlby C Blobfinder, a tool for fluorescence microscopy image cytometry. Comp. Meth. Prog. Biomed. 94 (2009) 58–65. 10.1016/j.cmpb.2008.08.006

[68]. Smith MA, Hall R, Fisher K, Haake SM, Khalil F, Schabath MB, Vuaroqueaux V, Fiebig HH, Altiok S, Chen YA, Haura EB Annotation of human cancers with EGFR signaling-associated protein complexes using proximity ligation assays. Sci. Signal. 8 (2015) ra4. 10.1126/scisignal. 2005906

[69]. Armour CL, Diment LM, Black JL Relationship between smooth muscle volume and contractile response in airway tissue. Isometric versus isotonic measurement. J. Pharmacol. Exp. Thera. 245 (1988) 687–691.

[70]. Meiss RA, Pidaparti RM Mechanical state of airway smooth muscle at very short lengths. J. Appl. Physiol. 96 (2004) 655–667. 10.1152/japplphysiol.00388.2003 [PubMed: 14594865]

[71]. Chitano P, Wang L, Tin GYY, Ikebe M, Pare PD, Seow CY Smooth muscle function and myosin polymerization. J Cell Sci. 130 (2017) 2468–2480. doi: 10.1242/jcs.202812. [PubMed: 28596242]

[72]. Pratusevich VR, Seow CY, Ford LE Plasticity in canine airway smooth muscle. J Gen Physiol. 105 (1995) 73–94. PMCID: PMC2216929 [PubMed: 7730790]

[73]. Gabella G The force generated by a visceral smooth muscle. J Physiol. 263 (1976) 199–213. PMCID: PMC1307697 [PubMed: 1018232]

[74]. Chen CP, Chen X, Qiao YN, Wang P, He WQ, Zhang CH, Zhao W, Gao YQ, Chen C, Tao T, Sun J, Wang Y, Gao N, Kamm KE, Stull JT, Zhu MS In vivo roles for myosin phosphatase targeting subunit-1 phosphorylation sites T694 and T852 in bladder smooth muscle contraction. J Physiol. 593 (2015) 681–700. 10.1113/jphysiol.2014.283853 [PubMed: 25433069]

[75]. Gao N, Chang AN, He W, Chen CP, Qiao YN, Zhu M, Kamm KE, Stull JT Physiological signaling to myosin phosphatase targeting subunit-1 phosphorylation in ileal smooth muscle. J Physiol. 594 (2016) 3209–3225. 10.1113/JP271703 [PubMed: 26847850]

[76]. Heerkens EH, Quinn L, Withers SB, Heagerty AM Beta integrins mediate FAK Y397 autophosphorylation of resistance arteries during eutrophic inward remodeling in hypertension. J. Vasc. Res. 51 (2014) 305–314. 10.1159/000365479 [PubMed: 25300309]

[77]. Li Y, Reznichenko M, Tribe RM, Hess PE, Taggart M, Kim H, DeGnore JP, Gangopadhyay S, Morgan KG Stretch activates human myometrium via Erk, caldesmon and focal adhesion signaling. PLoS One. 4 (2009) e7489 10.1371/journal.pone.0007489 [PubMed: 19834610]

[78]. Tang D, Mehta D, Gunst SJ Mechanosensitive tyrosine phosphorylation of paxillin and focal adhesion kinase in tracheal smooth muscle. Am. J. Physiol. 276 (1999) C250–C258. 10.1152/ajpcell.1999.276.1.C250 [PubMed: 9886941]

[79]. Zheng C, Xing Z, Bian ZC, Guo C, Akbay A, Warner L, Guan JL Differential regulation of Pyk2 and focal adhesion kinase (FAK). The C-terminal domain of FAK confers response to cell adhesion. J. Biol. Chem. 273 (1998) 2384–2389. 10.1074/jbc.273.4.2384 [PubMed: 9442086]

[80]. Corbalan-Garcia S, Gomez-Fernandez JC Classical protein kinases c are regulated by concerted interaction with lipids: The importance of phosphatidylinositol-4,5-bisphosphate. Biophys. Rev. 6 (2014) 3–14. 10.1007/s12551-013-0125-z

[81]. Miller NLG, Lawson C, Chen XL, Lim S-T, Schlaepfer DD Rgnef (p190rhogef) knockout inhibits Rhoa activity, focal adhesion establishment, and cell motility downstream of integrins. PloS One. 7 (2012) e37830 10.1371/journal.pone.0037830 [PubMed: 22649559]

[82]. Han Y, Wang X, Chen J, Sha SH Noise-induced cochlear F-actin depolymerization is mediated via ROCK2/p-Erm signaling. J. Neurochem. 133 (2015) 617–268. 10.1111/jnc.13061 [PubMed: 25683353]

[83]. Truebestein L, Elsner DJ, Fuchs E, Leonard TA A molecular ruler regulates cytoskeletal remodelling by the Rho kinases. Nat. Commun. 6 (2015) 10029 10.1038/ncomms10029 [PubMed: 26620183]

[84]. Wang S, Chen C, Su K, Zha D, Liang W, Hillebrands JL, Goor H, Ding G Angiotensin II induces reorganization of the actin cytoskeleton and myosin light-chain phosphorylation in podocytes through Rho/ROCK-signaling pathway. Ren. Fail. 38 (2016) 268–275. 10.3109/0886022X.2015.1117896 [PubMed: 26652313]

[85]. Khasnis M, Nakatomi A, Gumpper K, Eto M Reconstituted human myosin light chain phosphatase reveals distinct roles of two inhibitory phosphorylation sites of the regulatory subunit, mypt1. Biochemistry. 53 (2014) 2701–2709. 10.1021/bi5001728 [PubMed: 24712327]

[86]. Khromov A, Choudhury N, Stevenson AS, Somlyo A, Eto M Phosphorylation-dependent autoinhibition of myosin light chain phosphatase accounts for Ca^{2+} sensitization force of smooth muscle contraction. J Biol Chem. 284 (2009) 21569–21579. 10.1074/jbc.M109.019729. [PubMed: 19531490]

[87]. Velasco G, Armstrong C, Morrice N, Frame S, Cohen P Phosphorylation of the regulatory subunit of smooth muscle protein phosphatase 1d at thr850 induces its dissociation from myosin. FEBS Lett. 527 (2002) 101–104. PMID: 12220642 [PubMed: 12220642]

[88]. Case LB, Waterman CM Integration of actin dynamics and cell adhesion by a three-dimensional, mechanosensitive molecular clutch. Nat. Cell Biol. 17 (2015) 955–963. 10.1038/ncb3191 [PubMed: 26121555]

[89]. Goult BT, Yan J, Schwartz MA Talin as a mechanosensitive signaling hub. J. Cell Biol. 217 (2018) 3776–3784. 10.1083/jcb.201808061 [PubMed: 30254032]

[90]. Li Z, Lee H, Zhu C Molecular mechanisms of mechanotransduction in integrin-mediated cell-matrix adhesion. Exp. Cell Res. 349 (2016) 85–94. 10.1016/j.yexcr.2016.10.001 [PubMed: 27720950]

[91]. Critchley DR Biochemical and structural properties of the integrin-associated cytoskeletal protein talin. Ann. Rev. Biophys. 38 (2009) 235–254. 10.1146/annurev.biophys.050708.133744 [PubMed: 19416068]

[92]. Sun Z, Guo SS, Fassler R Integrin-mediated mechanotransduction. J. Cell Biol. 215 (2016) 445–456. 10.1083/jcb.201609037 [PubMed: 27872252]

[93]. Yao M, Goult BT, Klapholz B, Hu X, Toseland CP, Guo Y, Cong P, Sheetz MP, Yan J The mechanical response of talin. Nat. Comm. 7 (2016) 11966 10.1038/ncomms11966

Highlights

- in situ PLA quantitatively measured protein phosphorylation in small tissues.

- in situ PLA detected differences in smooth muscle protein phosphorylation responses.

- Myofilament calcium sensitization proteins relocate to β1integrin during contraction.

- FAK inhibition blocked contractile protein relocation to β1integrin.

- in situ PLA revealed myofilament reorganization at β1integrins.
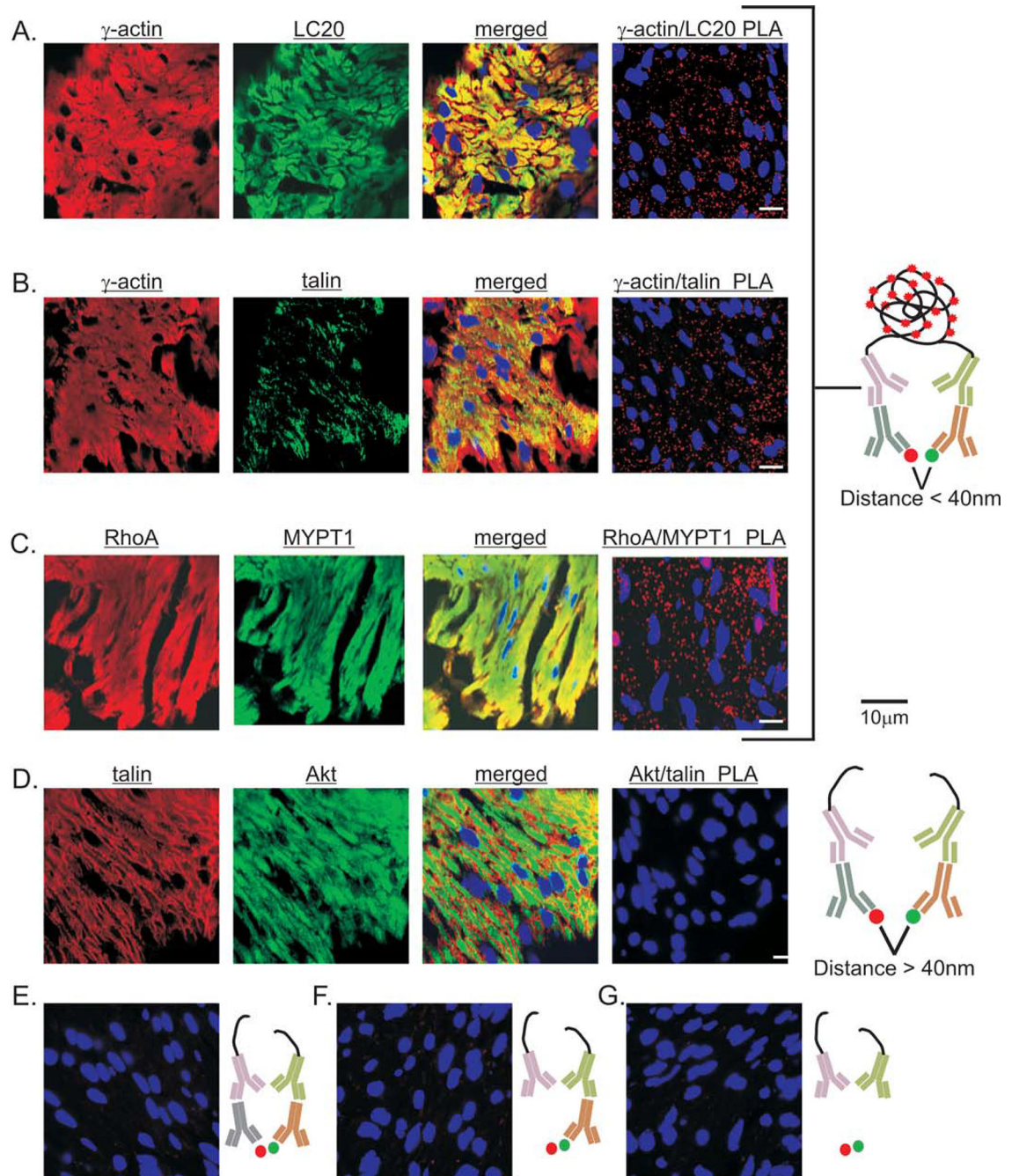
Figure 1. Positive and negative biological controls for PLA of smooth muscle tissue sections.
Representative images validating the anti-γ-actin, anti-LC20 (A), anti-talin (B), anti RhoA, anti-MYPT1 (C), and anti-Akt antibodies (D) by immunofluorescence. Image overlays of anti-γ-actin and anti-LC20 (A), anti-talin and anti-γ-actin (B), anti-RhoA and anti-MYPT1 (C), and anti-talin and anti-Akt (D). Representative PLA images of γ-actin/LC20 (A), γ-actin/talin (B), RhoA/MYPT1 (C), and talin/Akt (D). Schematic illustration of PLA positive (A,B,C) and negative (D) biological controls. Representative images of negative technical controls with its corresponding schematic illustration; (E) non-immune IgG paired with

single primary antibody (IgG/Akt PLA), (F) single primary antibody (blank/Akt PLA), and (G) only secondary PLA probes (no primary Abs PLA). Cell nuclei are labeled with DAPI (4',6-diamidino-2-phenylidole) (blue).
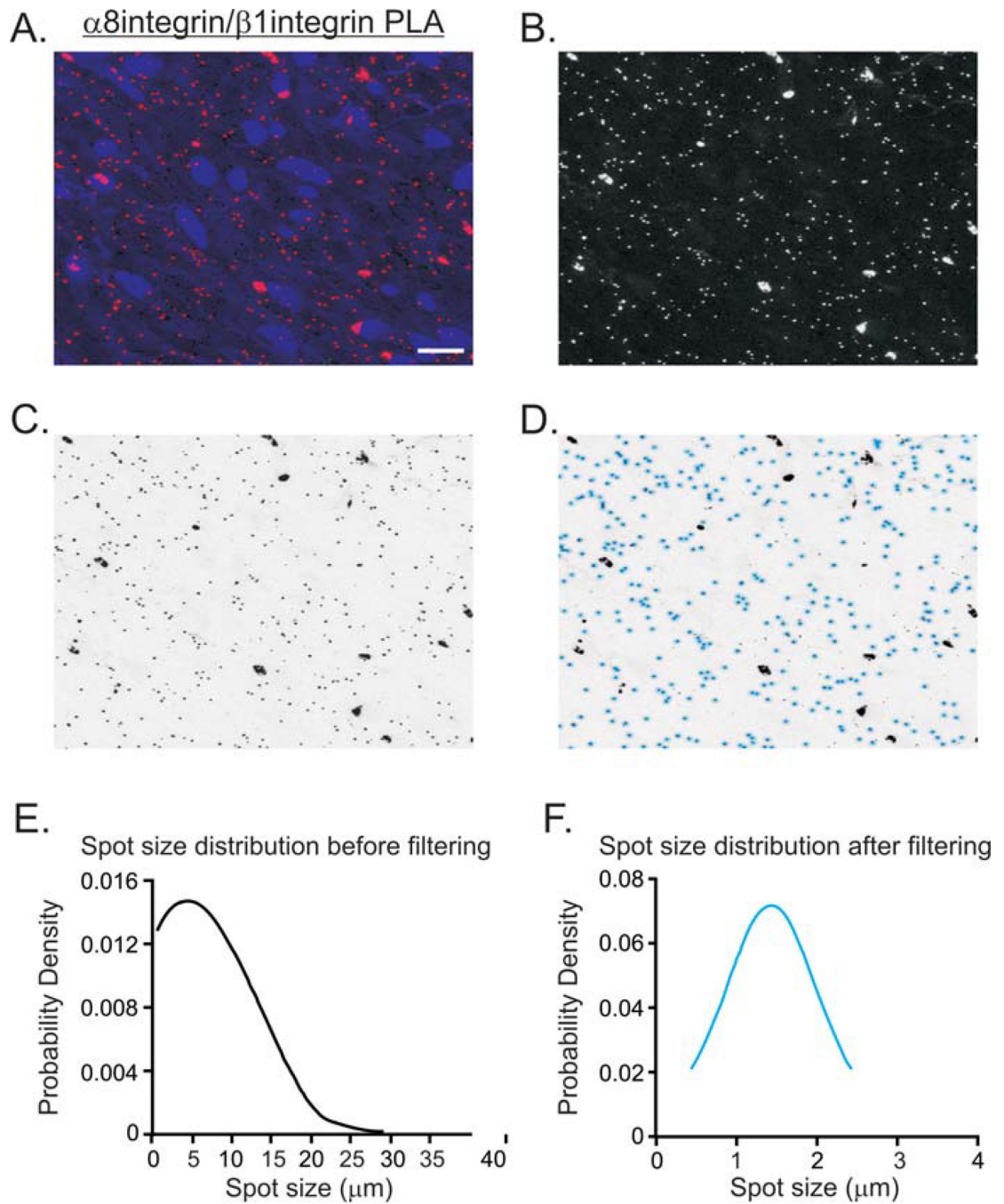
Figure 2. Thresholding and particle analysis of PLA spots from gastric fundus smooth muscle sections.

(A) Representative image of α8integrin/β1integrin PLA (red), and DAPI stained nuclei (blue). (B) The α8integrin/β1integrin PLA image with the red channel isolated and converted by Fiji. (C) Inverse of the image in B. (D) The image in C, processed for thresholding using Fiji default parameters. Real PLA spots are distinguished from the noise and circled with light blue. The PLA spot size distribution before filtering (E) and after filtering (F) by particle analysis. 228 and 162 spots were counted before and after filtering.
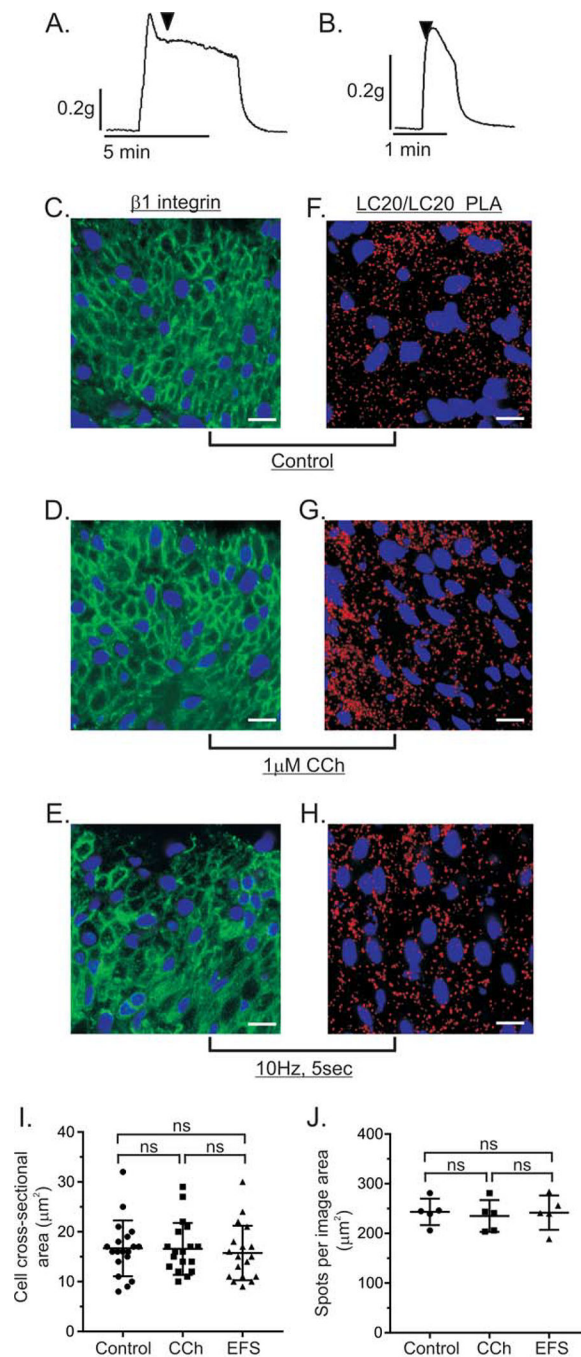
Figure 3. Internal standards for quantitation of PLA spots relative to cell density or LC20/LC20 isPLA.

Representative traces of the force generated by isometric contraction of murine gastric fundus smooth muscle strips in response to 1μM CCh (A), or 10Hz EFS (B). Arrowheads indicate the time point at which the strips were submerged into room temperature 4% (w/v) PFA. Representative images of β1integrin immunofluorescence from gastric fundus smooth muscles that were unstimulated (Control, n=3) (C), contracted by 1μM CCh, n=3 (D), or 10Hz EFS, n=3 (E). Representative images of LC20/LC20 PLA from unstimulated gastric fundus smooth muscles (Control, n=3) (F), contracted by 1μM CCh, n=3 (G), or 10Hz EFS,

n=3 (H). (I) Average ± SD of the cellular cross-sectional areas. (J) Average ± SD of the number of PLA spots per total image area. Cell nuclei were labeled with DAPI (blue).
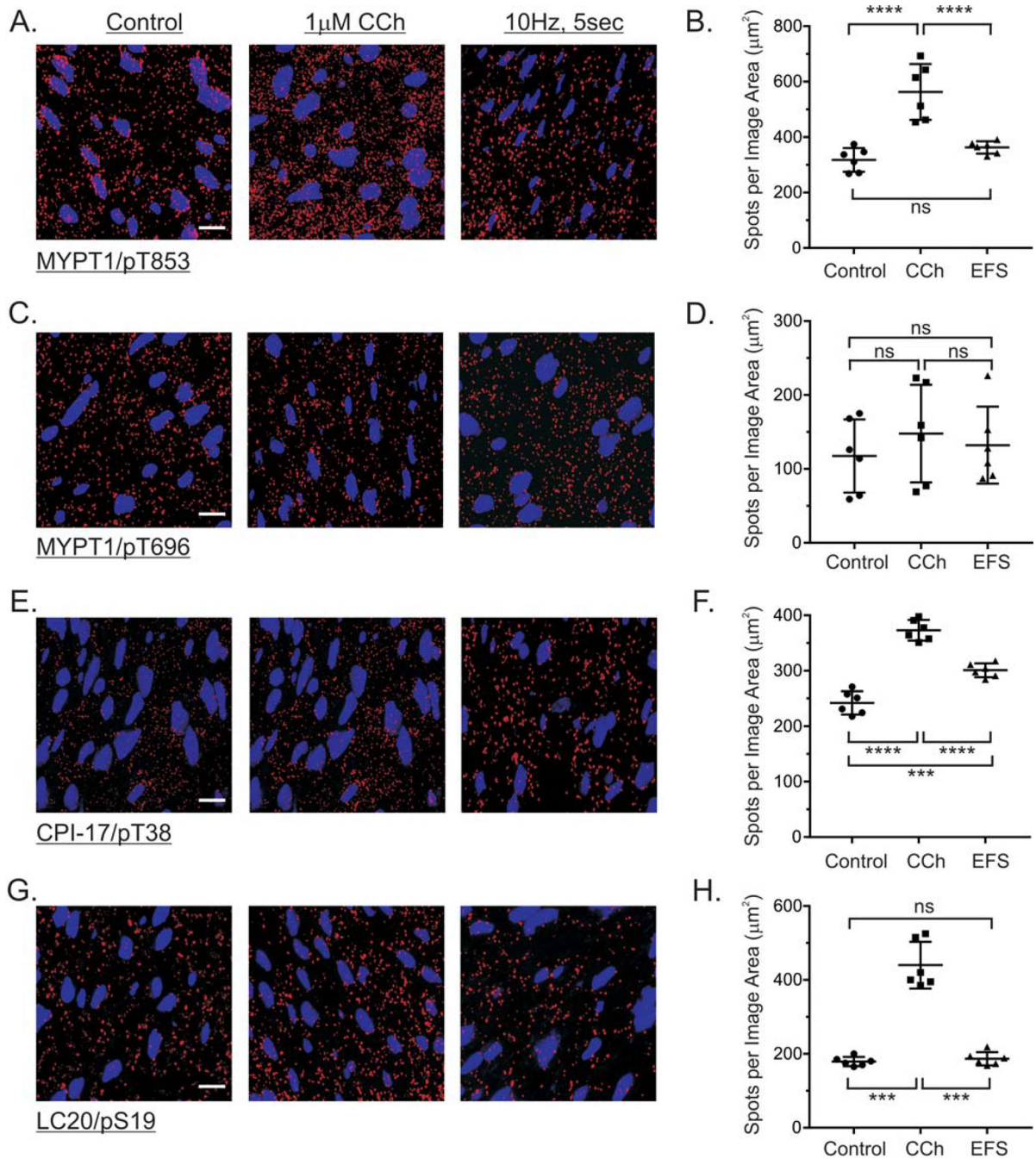
Figure 4. MYPT1, CPI-17, and LC20 phosphorylation in response to cholinergic stimulation of gastric fundus muscle strips.

Representative isPLA images and average ratios ± SD of MYPT1/pT853 (A, B), MYPT1/pT696 (C, D), CPI-17/pT38 (E, F), and LC20/pS19 (G, H) from muscles with no treatment (Control), 1μM CCh, 1min, in the presence of 0.3μM tetrodotoxin, and 10Hz, 5sec EFS in the presence of 100μM L-NNA and 1μM MRS2500. ***P<0.001, ****P<0.0001, ns P>0.05, n=3 for each treatment.
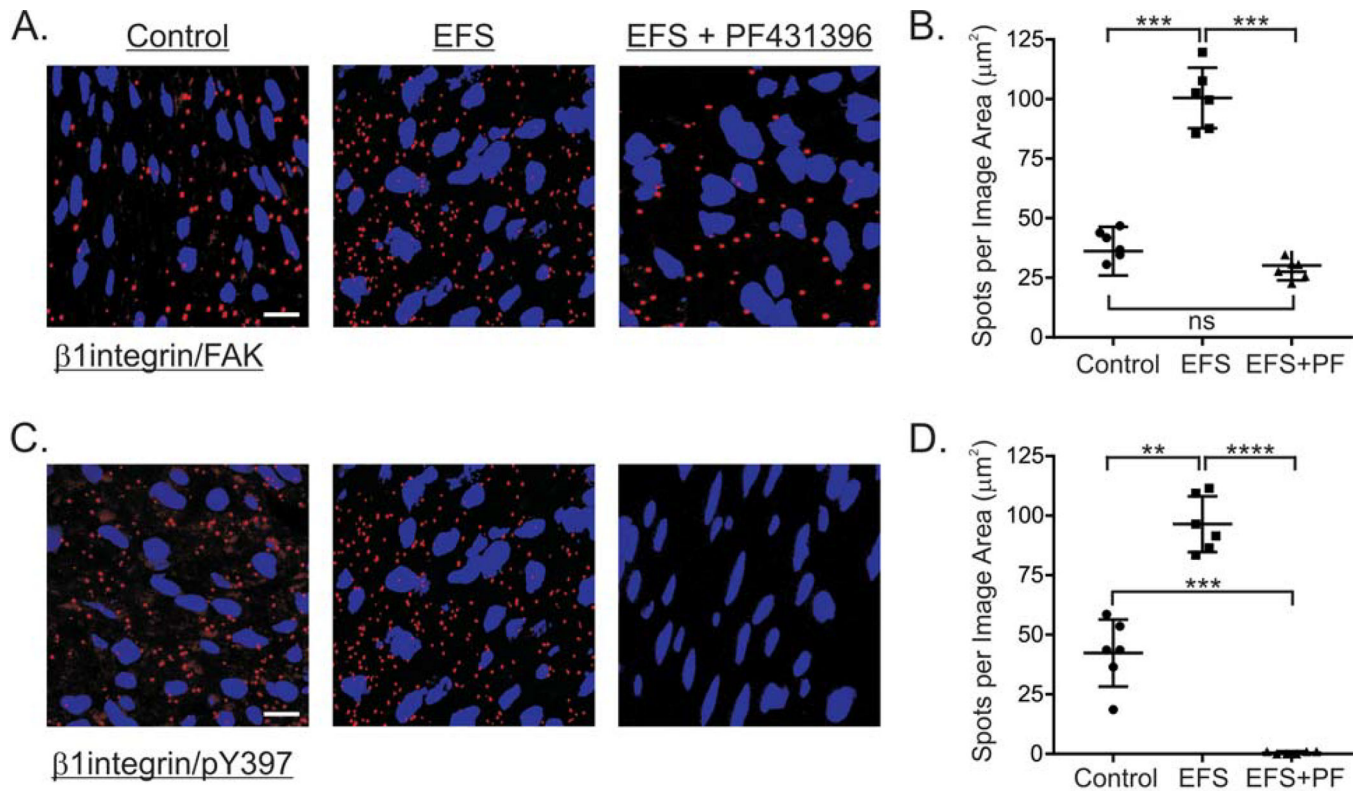
Figure 5. PF-431396 inhibits β1integrin and FAK association in response to EFS-evoked cholinergic neurotransmisssion of gastric fundus muscle strips.

Representative isPLA images and average ratios ± SD of β1integrin/FAK (A, B), and β1integrin/pY397 (C, D) from muscles with no treatment (Control), and (EFS) (10Hz, 5sec) in the presence of 100μM L-NNA and 1μM MRS2500, without, or with 1μM PF-431396. **P<0.01, ***P<0.001, ****P<0.0001, ns P>0.05, n=3 for each treatment.
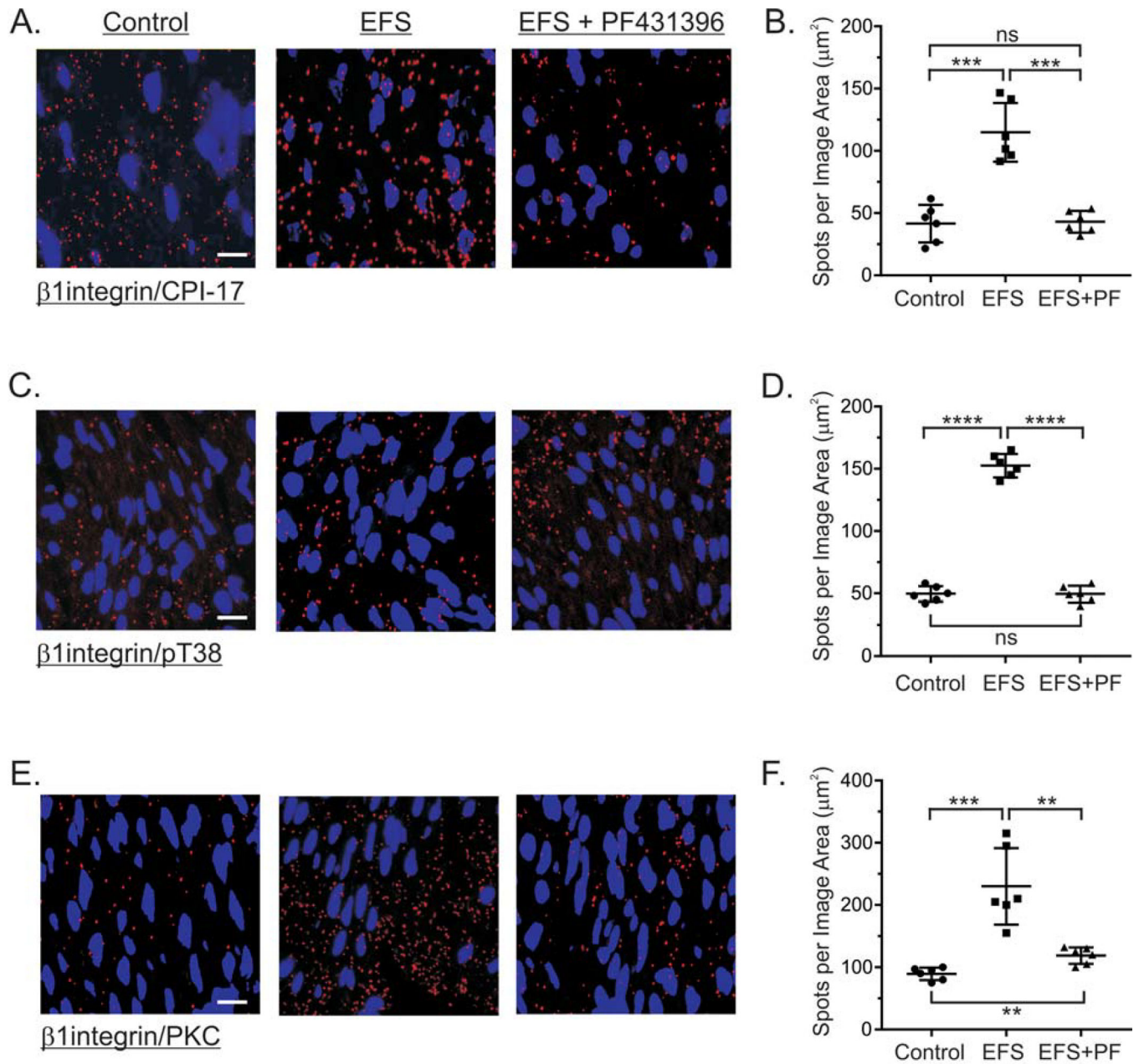
Figure 6. PF-431396 inhibits the association of CPI-17, phosphorylated CPI-17, and PKC with β1integrin in response to EFS-evoked cholinergic neurotransmisssion of gastric fundus muscle strips.

Representative isPLA images and average ratios ± SD of β1integrin/CPI-17 (A, B),

β1integrin/pT38 (C, D), and β1integrin/PKC (E, F) from muscles with no treatment

(Control), and (EFS) (10Hz, 5sec) in the presence of 100μM L-NNA and 1μM MRS2500,

without, or with 1μM PF-431396. **P<0.01, ***P<0.001, ****P<0.0001, ns P>0.05, n=3

for each treatment.
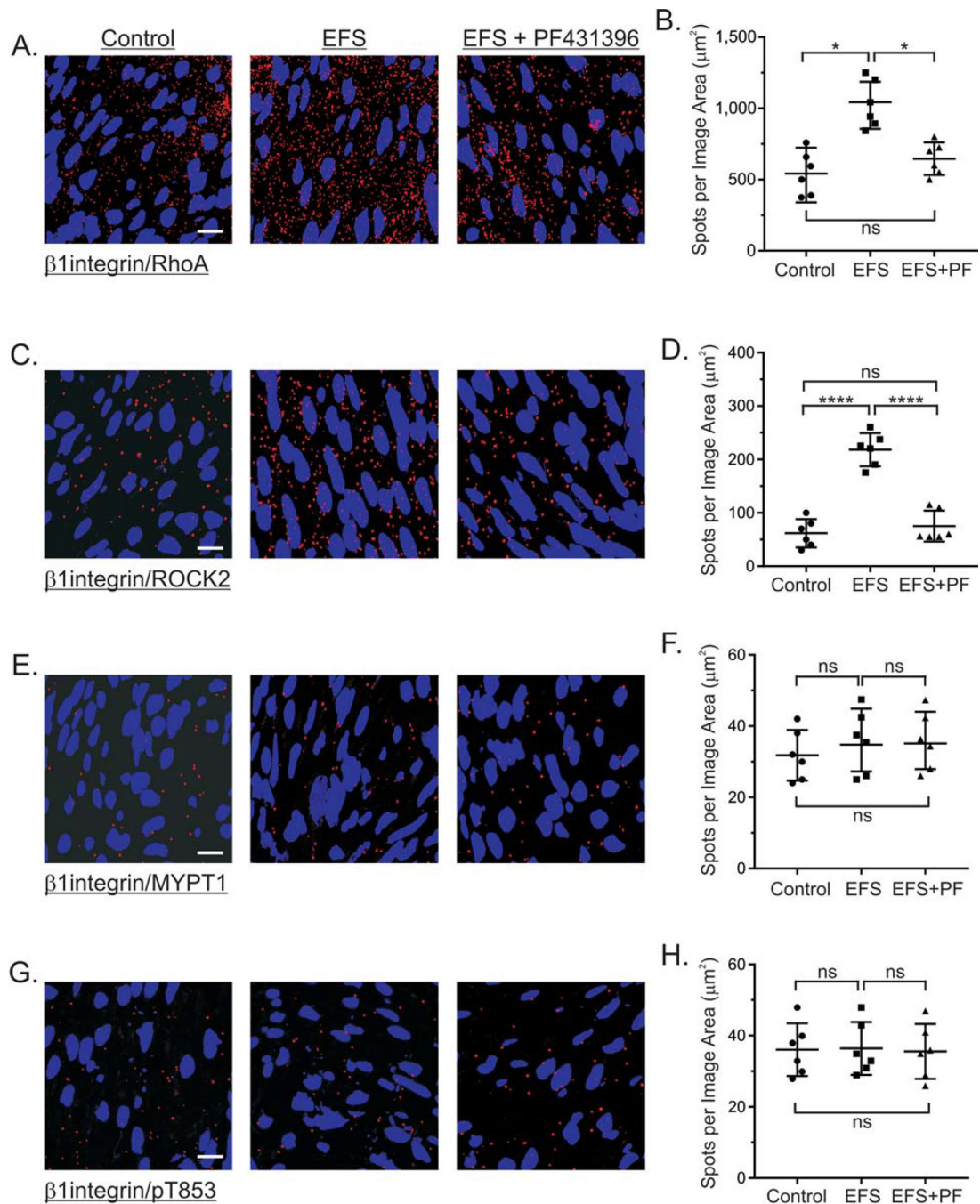
Figure 7. Effects of EFS-evoked cholinergic neurotransmisssion and PF-431396 on the association of RhoA, ROCK2, and MYPT1 with β1integrin.

Representative isPLA images and average ratios ± SD of β1integrin/RhoA (A, B), β1integrin/ROCK2 (C, D), and β1integrin/MYPT1 (E, F) and β1integrin/pT853 (G, H) from muscles with no treatment (Control), and (EFS) (10Hz, 5sec) in the presence of 100μM L-NNA and 1μM MRS2500, without, or with 1μM PF-431396. *P<0.05, ****P<0.0001, ns P>0.05, n=3 for each treatment.
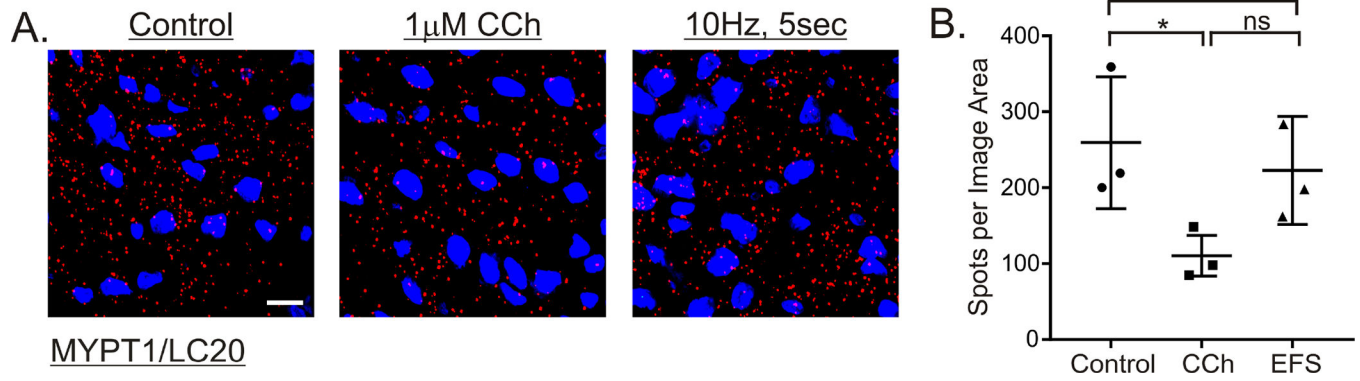
Figure 8. Effects of cholinergic stimulation on the association of MYPT1 with LC20.
Representative isPLA images and average ratios ± SD of MYPT1/LC20 (A, B) from
muscles with no treatment (Control), 1μM CCh, 1min, in the presence of 0.3μM
tetrodotoxin, and 10Hz, 5sec EFS in the presence of 100μM L-NNA and 1μM MRS2500.
*P<0.05, ns P>0.05, n=3 for each treatment.
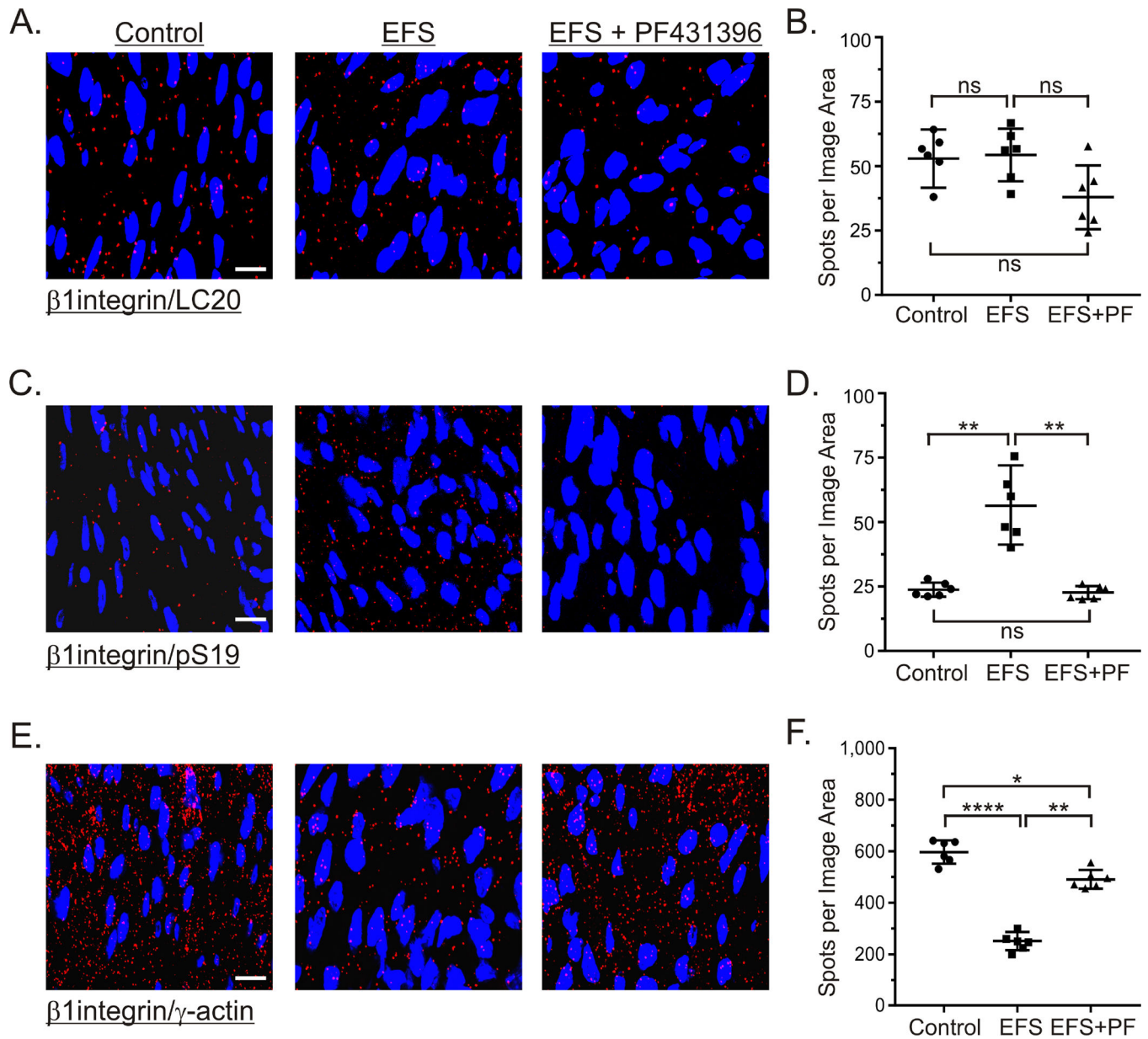
Figure 9. Effects of EFS-evoked cholinergic neurotransmisssion and PF-431396 on the association of LC20 and γ-actin with β1integrin.

Representative isPLA images and average ratios ± SD of β1integrin/LC20 (A, B), β1integrin/pS19 (C, D), and β1integrin/γ-actin (E, F) from muscles with no treatment (Control), and 10Hz, 5sec EFS in the presence of 100μM L-NNA and 1μM MRS2500, without, or with 1μM PF-431396. *P<0.05, **P<0.01, ****P<0.0001, ns P>0.05. n=3 for each treatment.